Fine-tuning the orientation of the polarity axis by Rga1, a Cdc42 GTPase-activating protein

Kristi E. Miller[a], Wing-Cheong Lo[b], Mid Eum Lee[a,†], Pil Jung Kang[c], and Hay-Oak Park[a,c,*]
[a]Molecular Cellular Developmental Biology Program and [c]Department of Molecular Genetics, The Ohio State University, Columbus, OH 43210; [b]Department of Mathematics, City University of Hong Kong, Kowloon, Hong Kong

ABSTRACT **In yeast and animal cells, signaling pathways involving small guanosine triphosphatases (GTPases) regulate cell polarization. In budding yeast, selection of a bud site directs polarity establishment and subsequently determines the plane of cell division. Rga1, a Cdc42 GTPase-activating protein, prevents budding within the division site by inhibiting Cdc42 repolarization. A protein complex including Nba1 and Nis1 is involved in preventing rebudding at old division sites, yet how these proteins and Rga1 might function in negative polarity signaling has been elusive. Here we show that Rga1 transiently localizes to the immediately preceding and older division sites by interacting with Nba1 and Nis1. The LIM domains of Rga1 are necessary for its interaction with Nba1, and loss of this interaction results in premature delocalization of Rga1 from the immediately preceding division site and, consequently, abnormal bud-site selection in daughter cells. However, such defects are minor in mother cells of these mutants, likely because the G1 phase is shorter and a new bud site is established prior to delocalization of Rga1. Indeed, our biphasic mathematical model of Cdc42 polarization predicts that premature delocalization of Rga1 leads to more frequent Cdc42 repolarization within the division site when the first temporal step in G1 is assumed to last longer. Spatial distribution of a Cdc42 GAP in coordination with G1 progression may thus be critical for fine-tuning the orientation of the polarity axis in yeast.**

Monitoring Editor
Rong Li
Johns Hopkins University

Received: Feb 7, 2017
Revised: Oct 19, 2017
Accepted: Oct 20, 2017

INTRODUCTION

Establishing cell polarity in a proper orientation is critical for development and cell proliferation (Drubin and Nelson, 1996; Nelson, 2003). In most fungal and animal cells, selection of a polarity axis is linked to polarity establishment via a conserved mechanism involving the Cdc42 GTPase (Johnson, 1999; Etienne-Manneville, 2004; Park and Bi, 2007). Cells of the budding yeast *Saccharomyces cerevisiae* grow by choosing a single bud site, which determines the axis of cell polarity and the plane of cell division. Bud-site selection occurs in a cell-type-specific manner (Freifelder, 1960; Hicks *et al.*, 1977; Chant and Pringle, 1995): **a** or α cells (such as wild-type haploids) bud in the axial pattern, in which a new bud site is chosen adjacent to the previous division site. In contrast, **a**/α cells (such as wild-type diploids) bud in the bipolar pattern, in which daughter cells typically bud at the pole distal from the division site, and mother cells choose a new bud adjacent to the division site or at the opposite pole. The axial pattern depends on a transient cortical marker that includes Bud3, Bud4, Axl1, and Axl2 (see Bi and Park, 2012). This axial landmark interacts with the Rsr1 GTPase module (Kang *et al.*, 2001; Kang *et al.*, 2012) composed of Rsr1 (also known as Bud1), its GTPase-activating protein (GAP) Bud2, and its guanine nucleotide exchange factor (GEF) Bud5 (Bender and Pringle, 1989; Chant and Herskowitz, 1991; Chant *et al.*, 1991; Park *et al.*, 1993). The Rsr1 GTPase module then interacts with Cdc42 and its GEF Cdc24 to couple the spatial cue to polarity establishment (Zheng *et al.*, 1995; Park *et al.*, 1997; Kozminski *et al.*, 2003; Kang *et al.*, 2010). Bud3 also directly activates Cdc42 in early G1, supporting a

This article was published online ahead of print in MBoC in Press (http://www.molbiolcell.org/cgi/doi/10.1091/mbc.E17-01-0074) on October 26, 2017.

†Present address: Department of Biochemistry and Cell Biology, The Geisel School of Medicine at Dartmouth, Hanover, NH 03755

*Address correspondence to: Hay-Oak Park (park.294@osu.edu).

Abbreviations used: FRAP, fluorescence recovery after photobleaching; GAP, GTPase-activating protein; GEF, guanine nucleotide exchange factor; GST, glutathione *S*-transferase; GTPase, guanosine triphosphatases; MBP, maltose-binding protein; PBD, p21-binding domain; PCC, Pearson's correlation coefficient; SIM, structured illumination microscopy; WT, wild type.

model that stepwise activation of Cdc42 is necessary for spatial cue-directed Cdc42 polarization (Kang *et al.*, 2014).

Both haploid and diploid cells select a new bud site that does not overlap with any previous bud site (Barton, 1950; Mortimer and Johnston, 1959; Hicks *et al.*, 1977; Chant and Pringle, 1995). Each cell division site on the mother cell surface is marked by a chitin-rich ring (called a "bud scar"), while the division site on the daughter cell is marked by a frail chitin-less structure (called a "birth scar") (Bacon *et al.*, 1966; Cabib and Bowers, 1971) (Figure 1A). The interdependent transmembrane proteins Rax1 and Rax2, which mark the cell division sites through multiple generations, are known to be involved in bipolar budding as the persistent pole marker in **a**/α cells (Chen *et al.*, 2000; Kang *et al.*, 2004). However, their role in the axial budding pattern had not been known when this study began. Here, the bud neck during cytokinesis is referred to as the current division site and is distinguished from the immediately preceding division site (i.e., the most recently used division site), at which Rax1 and Rax2 have arrived (Figure 1A).

Cdc42 and its GAP Rga1 are also involved in proper bud-site selection (Johnson and Pringle, 1990; Miller and Johnson, 1997; Stevenson *et al.*, 1995; Chen *et al.*, 1996; Smith *et al.*, 2002; Lo, Lee, *et al.*, 2013; Kang *et al.*, 2014). Interestingly, among Cdc42 GAPs, Rga1 is uniquely required for preventing budding within the previous division site by inhibiting Cdc42 repolarization (Tong *et al.*, 2007). A protein complex including Nba1 and Nis1, which interact with Rax1 and Rax2, has been suggested to inhibit Cdc42 at the old division sites (referred to as "cytokinesis remnants" [CRMs]) and thus function as negative polarity cues (Meitinger *et al.*, 2014). We recently found that Rga1 localizes to old division sites in addition to the current division site (Lee *et al.*, 2015). These observations raised a number of questions, including how Rga1 might localize to the old division sites and whether its function at these sites might be related to the negative polarity cues at CRMs. To address these questions, we combined various methods including quantitative microscopy and mathematical modeling. Here we report that Rga1 localizes to the old division sites transiently via interaction with Nba1 and Nis1.

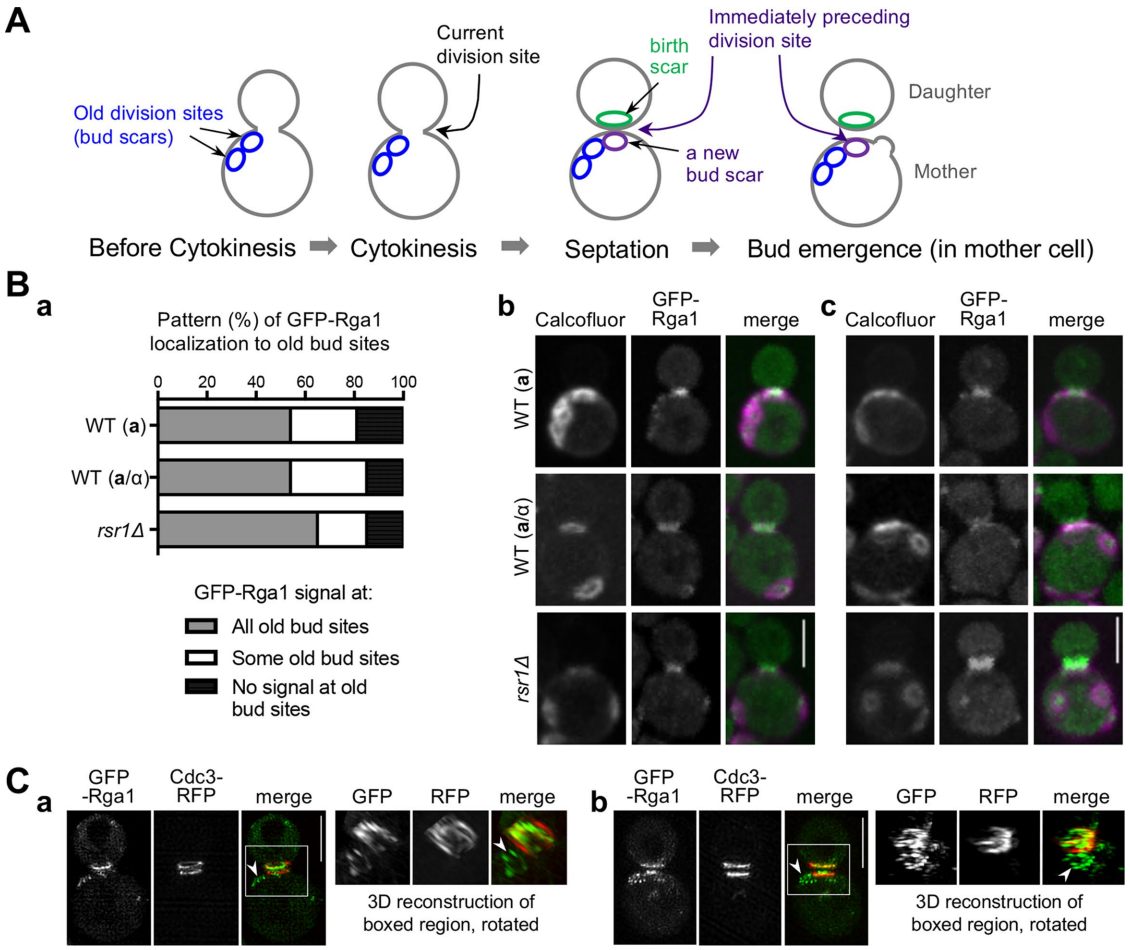

FIGURE 1: Localization of Rga1 to old cell division sites. (A) Scheme depicting the cell division sites in a yeast cell budding in the axial pattern. The current division site denotes the bud neck during cytokinesis. Following cytokinesis and cell separation, the division site becomes the most recently used site (i.e., the immediately preceding division site) and is marked with a new bud scar (purple) on the mother cell and with a birth scar (green) on the daughter cell. Older cell division sites on the mother cell are marked with bud scars (blue). (B) (a) Localization pattern of GFP-Rga1 to old bud sites is summarized from time-lapse images of cells budding in different patterns ($n = 26$ each strain). Representative images are shown for cells with GFP-Rga1 localized to all (b) or some (c) old bud sites. Bars, 3 μm. (C) Representative SIM images of GFP-Rga1 (marked with arrowhead at old bud site) and Cdc3-mCherry. Maximum intensity projection images (left) and three-dimensional reconstruction of boxed region (right) are shown for each cell. Bars, 3 μm.

We provide evidence that the Cdc42 GAP Rga1 is the core of negative polarity signaling at any previous cell division site.

RESULTS

Rga1 localizes to old division sites regardless of budding pattern

Although Cdc42 becomes enriched at the bud neck (which becomes the division site) in late M phase (Richman *et al.*, 2002), Rga1 inhibits Cdc42 activation and thus rebudding within the division site (Tong *et al.*, 2007). We thus asked whether Rga1 localizes only to old division sites that are adjacent to the bud neck (i.e., only in cells budding in the axial pattern) to inhibit Cdc42 repolarization at these sites. We examined localization of green fluorescent protein (GFP) tagged Rga1 in cells that bud in different patterns after staining with Calcofluor, which stains the bud scars and bud neck. We observed three different patterns of GFP-Rga1 localization in these cells (Figure 1B): GFP-Rga1 was present at all old bud sites (Figure 1Bb), some but not all old bud sites (Figure 1Bc), or none of the old bud sites. The percentage of these groups was not significantly different among wild-type (*WT*) **a** and **a**/α cells (which bud in an axial and a bipolar pattern, respectively) and *rsr1*Δ cells (which bud in a random pattern), indicating that Rga1 localizes to the old division sites of these cells regardless of their budding pattern. A close-up view of GFP-Rga1 by structured illumination microscopy (SIM) revealed that Rga1 localizes to the old division site as multiple dots organized as a ring (Figure 1C and Supplemental Video S1; $n = 4$).

Transient localization of Rga1 to the current and old division sites

How does Rga1 localize to old cell division sites? One possibility might be that Rga1 is inherited from the division site and then stably anchored at old division sites, as in the case of Rax1 and Rax2. Alternatively, Rga1 might localize to old cell division sites transiently in every cell cycle as it does to the current division site. To distinguish between these possibilities, we performed time-lapse imaging of *WT* haploid cells expressing GFP-Rga1 for one round of the cell division cycle. We observed that GFP-Rga1 at the immediately preceding division site disappeared around bud emergence in the next cell cycle (98%, $n = 52$ mother cells; 100%, $n = 32$ daughter cells). GFP-Rga1 at old division sites in mother cells also disappeared around bud emergence (96%, $n = 27$) and then reappeared at those sites during G2/M phase (89%, $n = 27$) (see arrowheads, Figure 2A).

We then compared dynamics of GFP-Rga1 at different stages of the cell cycle by fluorescence recovery after photobleaching (FRAP). We found that GFP-Rga1 at old bud sites was fairly dynamic with half-time of recovery ($t_{1/2}$) = 22.4 ± 1.6 s (Figure 2Ba). Similar dynamics were observed for GFP-Rga1 at the bud neck prior to cytokinesis and at the immediately preceding division site in early G1 (Figure 2B, b and d). GFP-Rga1 was most dynamic during cytokinesis (right after splitting of the Cdc3-RFP ring) ($t_{1/2}$ = 4.0 ± 1.8 s; Figure 2Bc). Taken together, these results indicate that Rga1 at the old division sites is dynamic, transiently arriving at these sites in each cell division cycle.

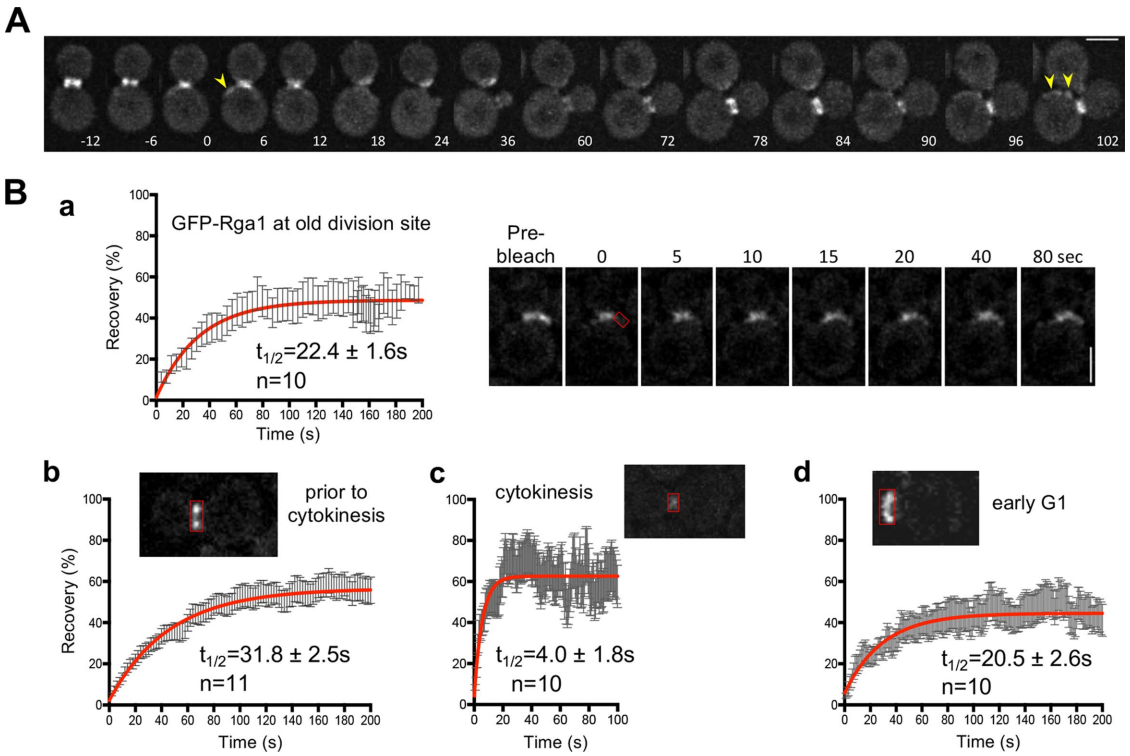

FIGURE 2: Rga1 is dynamic at old and current cell division sites. (A) GFP-Rga1 localizes to old bud site (marked with arrowheads) transiently in *WT* at 30°C. Numbers indicate time (in min) from the onset of cytokinesis ($t = 0$). Bar, 3 μm. (B) (a) FRAP analysis of GFP-Rga1 at old bud site. Left, recovery after photobleaching is plotted (mean ± SEM), and curve fit is in red. The half-time of recovery ($t_{1/2}$) (mean ± SEM) and number (n) of samples analyzed are shown. Right, representative cell before (prebleach) and after photobleaching. The red boxed region was bleached at time 0. Bar, 3 μm. (b–d) FRAP analysis of GFP-Rga1 at the bud neck prior to cytokinesis (b), during cytokinesis (c), and at the immediately preceding division site (d).

Localization of Rga1 to old division sites depends on Rax1, Rax2, Nis1, and Nba1

While Rga1 localization to the bud neck depends on septins (Caviston *et al.*, 2003), the "old" septin ring does not remain at the division site after G1 (Oh and Bi, 2011), suggesting that Rga1 relies on another protein(s) to localize to the old division sites. We considered a number of proteins that localize to old division sites as potential binding partners of Rga1. The persistent division site markers Rax1 and Rax2 arrive at the cell division site after septa formation (Chen *et al.*, 2000; Kang *et al.*, 2004; Khmelinskii *et al.*, 2012). Nba1 and Nis1, which initially localize to the current division site via the scaffold protein Gps1, also localize to the immediately preceding division site by interacting with Rax1/2 after septation and then remain at the old division sites for multiple generations (Meitinger *et al.*, 2014). We thus asked whether Rga1 is recruited to old division sites by these proteins. First, we found that GFP-Rga1 colocalized with Rax2-RFP, Nis1-RFP, and Nba1-RFP to the old and immediately preceding division sites (marked with arrowhead and arrows, respectively; mean Pearson's correlation coefficient, PCC > 0.5) (Figure 3A). We also tested whether

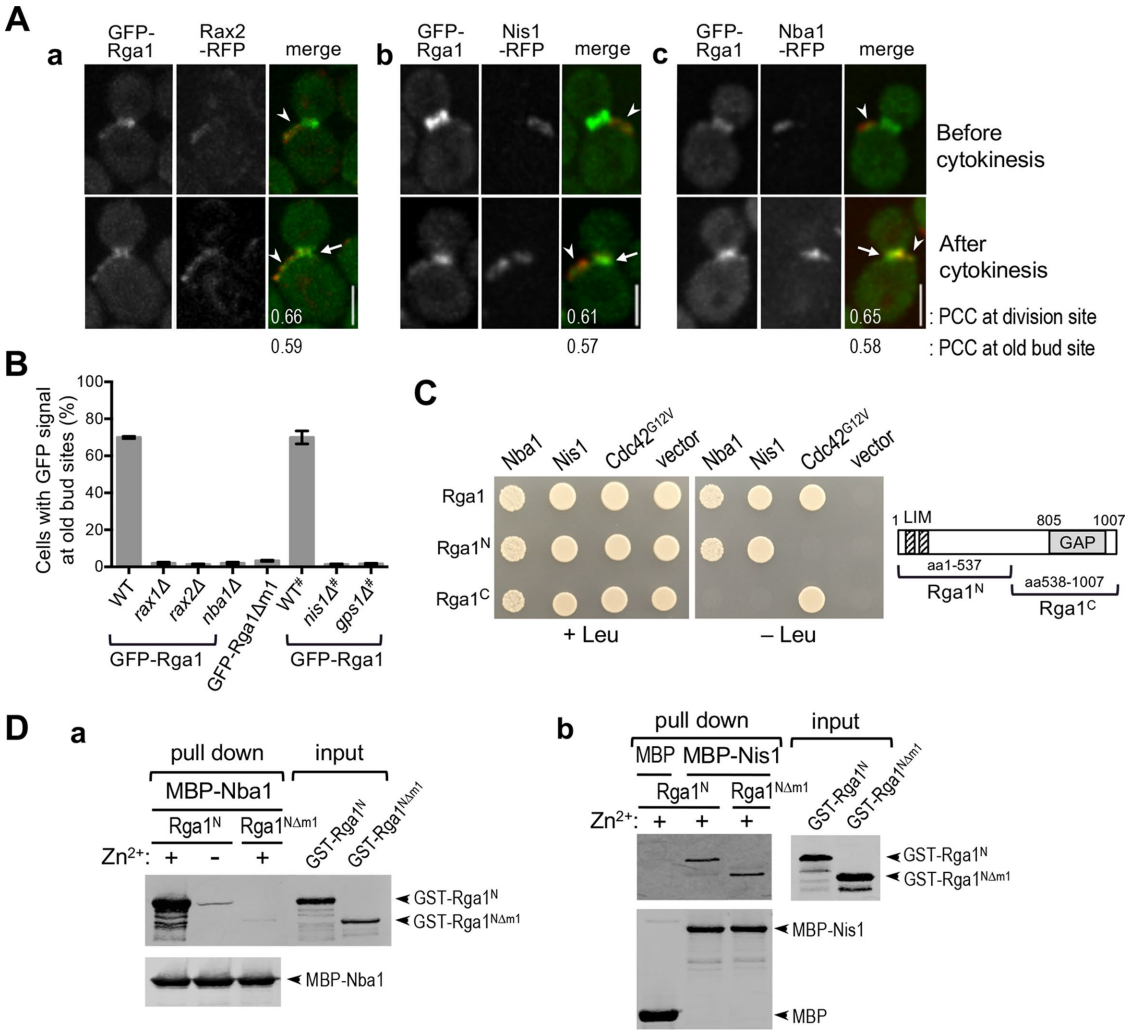

FIGURE 3: Localization of Rga1 to old bud sites depends on Rax1, Rax2, Nis1, and Nba1. (A) Colocalization of GFP-Rga1 with (a) Rax2-mCherry, (b) Nis1-tdTomato, and (c) Nba1-tdTomato. Numbers indicate mean PCC values at the immediately preceding division site (within images) and at older bud sites (below images). Number of cells analyzed for colocalization (at the immediately preceding division site and at the old division site) are as follows: Rax2 (31, 31); Nis1 (31, 31); and Nba1 (32, 25). Arrowheads and arrows mark old division sites and the immediately preceding division site, respectively. Bars, 3 μm. (B) Quantification of cells with GFP-Rga1 or GFP-Rga1Δm1 present at old bud sites. Strains marked with # are congenic to ESM356-1. Only large budded cells with old bud site(s) were counted. Mean ± SEM is shown from three independent experiments with the following total number of cells analyzed: *WT* (301), *rax1*Δ (311), *rax2*Δ (308), *nba1*Δ (322), *GFP-rga1Δm1* (300), *WT*# (396), *nis1Δ*# (338), and *gps1Δ*# (324). (C) Yeast two-hybrid assays of full-length and the truncated forms of Rga1 (depicted on the right). Growth on the –Leu plate denotes interaction. (D) MBP pull-down assays using MBP-Nba1 (a) and MBP-Nis1 (b) with the addition of extracts containing either GST-Rga1^{N} or GST-Rga1$^{N\Delta m1}$ in the presence or absence of Zn^{++}, as indicated. GST- and MBP-fusion proteins were detected with anti-GST and anti-MBP antibodies, respectively. Average recovery of GST-Rga1^{N} pulled down with MBP-Nba1 was 4% or 0.09% in the presence or absence of Zn^{+2}, respectively, and 0.08% GST-Rga1$^{N\Delta m1}$ was recovered with MBP-Nba1 in the presence of Zn^{+2}. Average recovery of GST-Rga1^{N} or GST-Rga1$^{N\Delta m1}$ with MBP-Nis1 was about the same (0.2%). No detectable GST-Rga1^{N} or GST-Rga1$^{N\Delta m1}$ was pulled down with MBP control.

localization of GFP-Rga1 to old bud sites was dependent on *RAX1, RAX2, NIS1*, or *NBA1* by examining large-budded cells of WT or mutants deleted for each of these genes after Calcofluor staining. We found that very few of these mutant cells (all of which express *GPS1*) had GFP-Rga1 localization to old division sites. Similarly, GFP-Rga1 localization to old division sites was not observed in *gps1*Δ cells (Figure 3B), likely because Nis1 and Nba1 were not initially recruited to the division site in the absence of Gps1 and thus were not present at the old division sites, as expected from the previous report (Meitinger *et al.*, 2014). These results are consistent with the idea that Rga1 is recruited to the old division site by Nba1 and Nis1, which themselves are anchored by Rax1 and Rax2.

The LIM domains of Rga1 are necessary for its interaction with Nba1

Since it had been suggested that Nba1 and Nis1 function as negative polarity cues independently from Rga1 (Meitinger *et al.*, 2014), it was surprising to find that Rga1 localization depends on Nba1 and Nis1. To explore this issue further, we examined whether Rga1 interacted with Nba1 and/or Nis1 by a yeast two-hybrid assay. We expressed Rga1 fused to a DNA-binding domain and Nba1 (or Nis1) fused to an activation domain in a strain carrying the *LEU2* reporter. Growth on a plate lacking Leu indicated that Rga1 interacts with Nba1 and Nis1, similarly to the positive control $Cdc42^{G12V}$ (which is expected to be the GTP-locked state in vivo and thus to interact with its GAP). Interestingly, when we tested truncated Rga1 fusion proteins, the N-terminal half of Rga1 (amino acids 1–537; $Rga1^{N}$) exhibited a similar two-hybrid interaction with Nba1 and Nis1. In contrast, the C-terminal fragment ($Rga1^{C}$), which carries the GAP domain, interacted with $Cdc42^{G12V}$ but not with Nba1 or Nis1 (Figure 3C). These results suggest that the N-terminal region of Rga1 specifically interacts with Nba1 and Nis1.

The N-terminal region of Rga1 contains tandem LIM domains (amino acids 1–122) (Chen *et al.*, 1996), which are named after their initial discovery in the proteins Lin11, Isl-1, and Mec-3. LIM domains are characterized by a unique cysteine-rich motif with a zinc-finger structure that often functions as a protein-binding interface (Kadrmas and Beckerle, 2004). Interestingly, it has been reported that Rga1 LIM domain mutants exhibit an abnormal budding pattern (Chen *et al.*, 1996). We thus postulated that the LIM domains of Rga1 might be involved in interaction with Nba1 and/or Nis1. To test this idea, we performed in vitro binding assays using recombinant proteins. $Rga1^{N}$ or $Rga1^{N\Delta m1}$ (which lacks LIM domains; denoted Δm1) was expressed as a glutathione *S*-transferase (GST) fusion protein, and Nba1 or Nis1 was expressed as an maltose binding protein (MBP) fusion protein from *Escherichia coli*. We found that MBP-Nba1 associated efficiently with GST-$Rga1^{N}$ but not GST-$Rga1^{N\Delta m1}$ in the MBP pull-down assay. Moreover, this $Rga1^{N}$-Nba1 association was dependent on the presence of Zn^{+2} (Figure 3Da), indicating that the LIM domains of Rga1 are indeed necessary for its interaction with Nba1. MBP-Nis1 associated similarly with both $Rga1^{N}$ and $Rga1^{N\Delta m1}$ in vitro (Figure 3Db), suggesting that another region in $Rga1^{N}$ is involved in interaction with Nis1.

We then examined how LIM domains might be involved in localization of GFP-Rga1 to old cell division sites by introducing the same LIM domain deletion mutation (Δm1). GFP-Rga1Δm1 poorly localized to old division sites in large budded cells, despite its localization to the bud neck (Figure 3B; see Figure 8 later in this article). Together, these results suggest that Rga1 localizes to old division sites via interaction with Nba1 and that the LIM domains of Rga1 are necessary for its interaction with Nba1.

Rga1 at the immediately preceding division site and older division sites may affect the orientation of the polarity axis

If Rga1 functions to prevent Cdc42 repolarization at old division sites, as it does at the current division site (Tong *et al.*, 2007), then we would predict that *rax1*Δ, *rax2*Δ, *nba1*Δ, and *nis1*Δ mutants exhibit improper bud-site selection. To test this idea, we examined the division sites of these mutants by staining cells with Calcofluor and wheat germ agglutinin conjugated to fluorescein isothiocyanate (WGA-FITC). WGA-FITC stains the division site in daughter cells (i.e., "birth scar") as well as bud scars in mother cells (see Figure 1A). Almost all daughter cells of *rax1*Δ, *rax2*Δ, *nba1*Δ, and *nis1*Δ mutants budded within the birth scar (marked with an arrow; Figure 4A). The majority of mother cells of these mutants had bud scars that often appeared adjacent to one another, although these bud scars (or a bud) were present within the birth scar (Figure 4B, ii). A smaller percentage of mutant mother cells had bud scars (or a bud) within a bud scar (Figure 4B, iii) or at the opposite poles (Figure 4B, iv), and these bud scars were also present within the birth scar. These analyses indicate that *rax1*Δ, *rax2*Δ, *nba1*Δ, and *nis1*Δ mutants are severely defective in selecting the first bud site, whereas subsequent budding events are partially defective.

Because there was some difficulty visualizing bud scars within a bud scar from the static images, we took a complementary approach to determine the role of Rga1 at the old division sites. We monitored Cdc42 polarization in *rax1*Δ cells by time-lapse imaging using the p21-binding domain of Gic2 fused to tdTomato (PBD-RFP), a biosensor for active Cdc42, which specifically interacts with Cdc42-GTP (Ozbudak *et al.*, 2005; Tong *et al.*, 2007; Okada *et al.*, 2017). The transcriptional repressor Whi5 fused to GFP was used as a cell-cycle marker, since its nuclear exit divides the G1 phase into two temporal steps, T_1 and T_2 (Di Talia *et al.*, 2007). In addition, Cdc3-GFP was used as both a cell-cycle and positional marker, since the septin hourglass splits into a double ring at the division site around the onset of cytokinesis (Kim *et al.*, 1991; Lippincott *et al.*, 2001). The PBD-RFP signal peaks at the presumptive bud site prior to disassembly of the septin ring at the division site, approximately concurrent with the appearance of new septin clouds (Okada *et al.*, 2013; Kang *et al.*, 2014; Lee *et al.*, 2015). Cdc42 always polarized at a site adjacent to the septin ring in mother and daughter cells of WT haploids (Figure 5B and Supplemental Figure S1), as expected. In contrast, Cdc42 polarized within the septin ring in a subset of *rax1*Δ mother cells (9.7%, $n = 31$; Figure 5B and Supplemental Figure S2B) and in the majority of *rax1*Δ daughter cells (Figure 5). This relatively minor defect of Cdc42 polarization in *rax1*Δ mother cells is thus consistent with the budding pattern (see Figure 4B).

We then employed mathematical modeling to simulate how Rga1 localization to the old bud site affects Cdc42 polarization. We extended our previous generic model of Cdc42 polarization on a two-dimensional computational domain with the axial landmark ring in the center (Figure 6A). This model incorporated two temporal steps in G1—the first step included positive feedback and delayed negative feedback, whereas the second step included stronger positive feedback with diminished negative feedback (Lee *et al.*, 2015). When Rga1 distribution at the current division site and at the previous division site (adjacent to the current division site) was implemented, our simulations showed that Cdc42 always polarized to a site that was outside of the old division site (Figure 6B, a and c). In contrast, if Rga1 was absent at the old division site, one of 10 simulations resulted in Cdc42 polarization within the old division site (Figure 6B, b and d), consistent with a minor defect in Cdc42 polarization in vivo (see Figure 5B). Collectively, both experimental data and computational modeling suggest that Rga1 localization to the

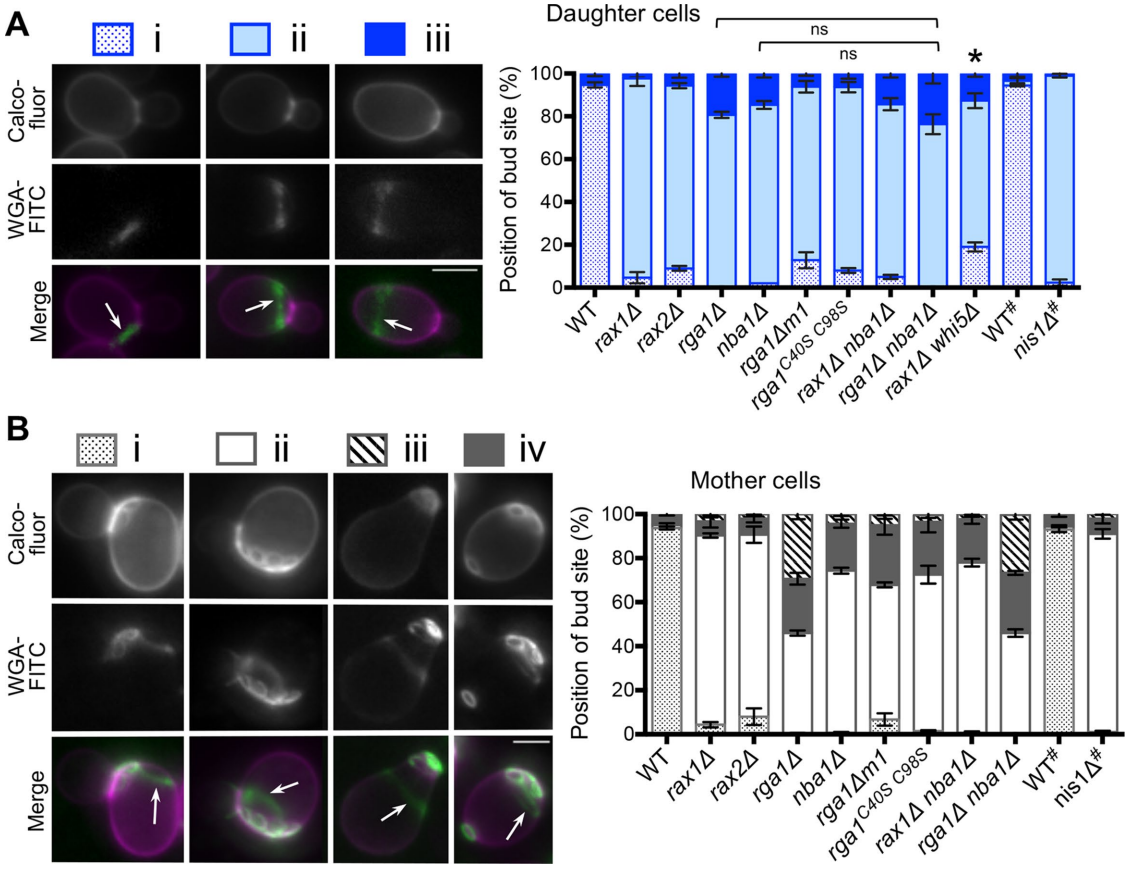

FIGURE 4: Bud-site selection of daughter and mother cells. Left, a representative image of each pattern is shown. Arrows mark birth scars. Bar, 3 μm. Right: Budding patterns (mean ± SEM) are plotted from three independent countings. Strains marked with # are congenic to ESM356-1. (A) The first bud position (purple) relative to birth scar (green) in daughter cells: (i) bud neck adjacent to the birth scar, (ii) bud neck within the birth scar, and (iii) bud neck at the opposite pole of birth scar. Total number of daughter cells counted: *WT* (257), *rax1*Δ (261), *rax2*Δ (274), *rga1*Δ (263), *nba1*Δ (260), *rga1*Δ*m1* (165), *rga1*$^{C40S\ C98S}$ (264), *rax1*Δ *nba1*Δ (238), *rga1*Δ *nba1*Δ (283), *rax1*Δ *whi5*Δ (351), *WT*$^{\#}$ (243), and *nis1*Δ$^{\#}$ (305). *$p = 0.01$ for *t* test comparing the axial pattern in *rax1*Δ vs. *rax1*Δ*whi5*Δ, and $p > 0.2$ for *rga1*Δ *nba1*Δ vs. *rga1*Δ and *rga1*Δ *nba1*Δ vs. *nba1*Δ; ns, not significant; $p > 0.05$. (B) Budding pattern of mother cells: (i) bud scars and bud neck adjacent to the birth scar (i.e., axial pattern), (ii) bud scar(s) and bud neck within the birth scar, (iii) bud scars (or a bud) within a bud scar (that is also within the birth scar), and (iv) bud scars or bud neck within the birth scar and at the opposite pole of the cell (i.e., a variation of the bipolar pattern). Total number of mother cells counted: *WT* (265), *rax1*Δ (269), *rax2*Δ (310), *rga1*Δ (323), *nba1*Δ (349), *rga1*Δ*m1* (239), *rga1*$^{C40S\ C98S}$ (256), *rax1*Δ *nba1*Δ (268), *rga1*Δ *nba1*Δ (407), *WT*$^{\#}$ (254), and *nis1*Δ$^{\#}$ (323).

immediately preceding division site and older division sites is important for inhibiting Cdc42 repolarization at these sites. However, having Rga1 activity at older division sites in mother cells may be less critical than at the current division site (see below for more discussion).

Mutational analyses suggest Rga1 functions in the same pathway with Nba1 and Nis1

Our data described so far support the idea that Rga1 functions together with Nba1 and Nis1. To explore further the functional interaction between Rga1 and these negative polarity cues, we asked whether improper bud-site selection of *rax1*Δ, *rax2*Δ, *nba1*Δ, and *nis1*Δ mutants was caused by their inability to recruit Rga1 to the previous division sites. To this end, we examined the *rga1*Δ*m1* mutant, because this LIM domain deletion disrupted the interaction between Rga1^{N} and Nba1 in vitro, and GFP-Rga1Δm1 poorly localized to the old bud sites in large-budded cells (see Figure 3, B and Da). It is noteworthy that the LIM domain mutant *rga1*$^{C40S\ C98S}$ (=*dbm1-5,7*) has been shown to exhibit an abnormal budding pattern (Chen *et al.*, 1996). Indeed, we found that the budding phenotypes of *rga1*Δ*m1* and *rga1*$^{C40S\ C98S}$ were very similar to those observed in mother and daughter cells of *rax1*Δ, *rax2*Δ, *nis1*Δ, and, in particular, an *nba1*Δ mutant (Figure 4). These observations suggest that the Rga1 LIM domain mutant protein, which poorly interacts with Nba1, is unable to promote proper bud-site selection. With the same logic, *rax1*Δ, *rax2*Δ, *nis1*Δ, and *nba1*Δ mutants exhibit improper bud-site selection, likely because Rga1 is not recruited to the previous division sites in these mutants.

If Rga1 and Nba1 function independently of each other to inhibit Cdc42 repolarization, as previously suggested (Meitinger *et al.*, 2014), then we would expect that a *rga1*Δ *nba1*Δ double mutant might have an additive budding defect compared with each single mutant. Remarkably, the pattern of bud positions of *rga1*Δ *nba1*Δ daughter cells was almost identical to that of *rga1*Δ or *nba1*Δ daughters. Indeed, no statistically significant difference was observed between daughter cells of these mutants with

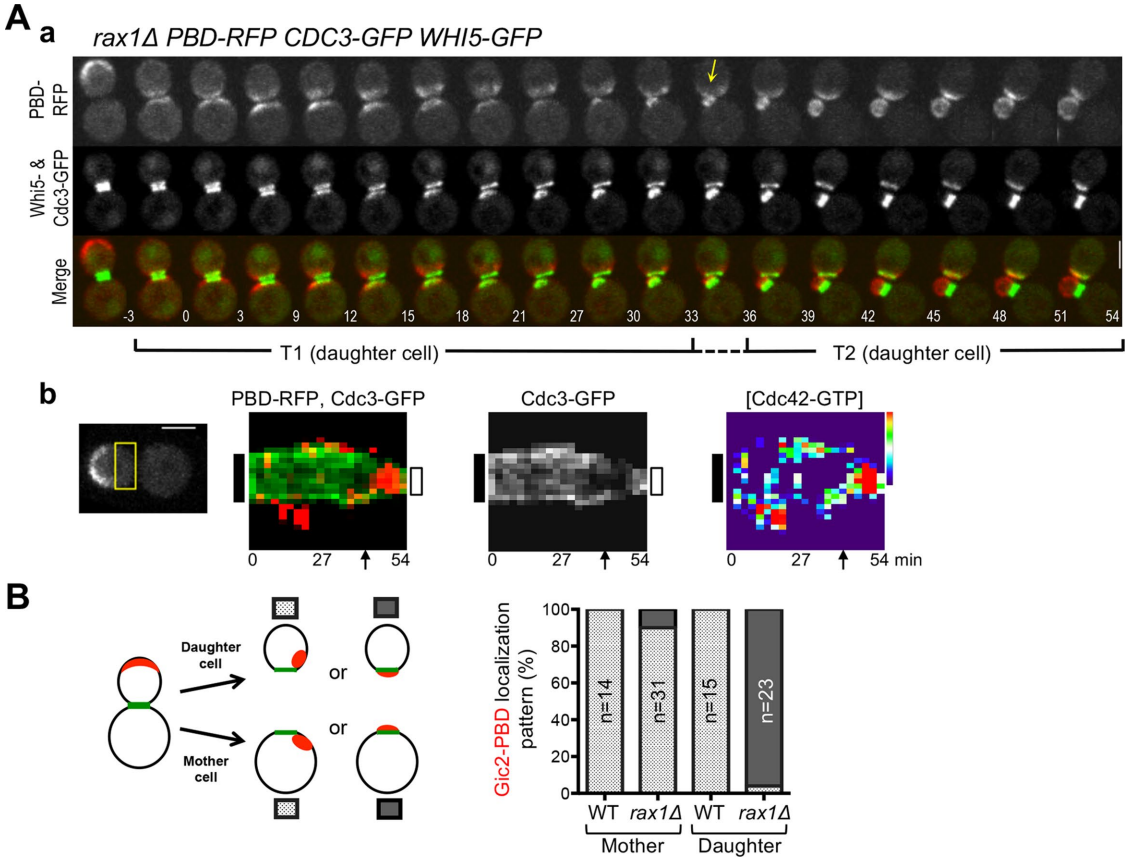

FIGURE 5: Cdc42 polarization in *rax1*Δ cells. (A) (a) Time-lapse images of PBD-RFP, Cdc3-GFP, and Whi5-GFP in *rax1*Δ cells at 30°C. Numbers indicate time (in min) from the onset of cytokinesis ($t = 0$). Yellow arrow indicates the time when the Cdc42 polarization axis becomes stabilized within the old septin ring. Bar, 3 μm. (b) Kymograph shows distribution of PBD-RFP and Cdc3-GFP (or Cdc3-GFP alone) in the region marked by a rectangle (size 1.73 × 3.89 μm) in the daughter cell. A heat map represents the Cdc42-GTP level of the kymograph shown on the left. The black and white bars on the sides of kymograph mark the position of the old and new septin rings, respectively. Note: New septin ring appears at the same position as the old septin ring in *rax1*Δ daughter cell. Arrows mark the T_1/T_2 boundary. (B) Localization pattern of Gic2-PBD-RFP (red) relative to the old septin ring (green) at the division site is quantified from a number (*n*) of time-lapse images. Mother cells of WT and *rax1*Δ are analyzed from time-lapse images taken at 22°C (see Supplemental Figures S1 and S2B).

respect to the percentage of budding within the birth scar (Figure 4A). The budding patterns of the *rga1*Δ *nba1*Δ mother cells were also similar to those of *rga1*Δ mother cells, while the defect was slightly less severe in *nba1*Δ mother cells (Figure 4B). Therefore, these data strongly support the idea that Rga1 functions in the same pathway with Nba1 and Nis1 at the previous division sites, rather than in a parallel pathway, to inhibit Cdc42 polarization.

Rga1 localizes to the immediately preceding division site via interaction with Nba1

As described above, almost all daughter cells of *rax1*Δ, *rax2*Δ, *nba1*Δ, and *nis1*Δ bud within the birth scar, while subsequent budding events in mother cells of these mutants are only partially defective. What could account for this difference between mother and daughter cells of these mutants? To address this question, we performed a series of time-lapse imaging and compared localization of GFP-Rga1, together with Whi5-RFP, in mother and daughter cells. We found that GFP-Rga1 remained at the immediately preceding division site almost until bud emergence in mother cells of *WT*, *nba1*Δ, and *rax1*Δ (100%, $n = 21$, *WT* and *rax1*Δ; 96%, $n = 28$, *nba1*Δ; Figure 7A and Supplemental Figure S2A). In contrast, localization of GFP-Rga1 in daughter cells of these mutants was clearly different compared with *WT* daughter cells. While GFP-Rga1 delocalized at the immediately preceding division site during T_2 in *WT* daughter cells (100%, $n = 21$; Figure 7Aa), GFP-Rga1 delocalized before transition to T_2 in *rax1*Δ daughter cells (83%, $n = 18$; Supplemental Figure S2A). GFP-Rga1 delocalized even earlier in *nba1*Δ daughter cells: 71% during T_1 and 29% at T_1/T_2 transition ($n = 17$; Figure 7, Ab and Bb). Local intensity of GFP-Rga1 at the immediately preceding division site was indeed significantly lower at the T_1/T_2 boundary in *nba1*Δ and *rax1*Δ daughter cells compared with *WT* daughter cells (Figure 7Bb). However, the global intensity and local intensity of GFP-Rga1 (at the bud neck) before cytokinesis were similar in all these strains (Figure 7B, a and b). The duration of T_1 and T_2 was also about the same among daughter cells of these strains (Figure 7Bc). Since Rga1 delocalizes earlier in *nba1*Δ daughter cells even during T_1, Rga1 may interact with Nba1 prior to interacting with other proteins at the immediately preceding division site.

To confirm that premature delocalization of Rga1 from the immediately preceding division site in these mutants is indeed due to lack of interaction between Rga1 and Nba1, we imaged GFP-Rga1Δm1, which lacks the LIM domains. Indeed, GFP-Rga1Δm1

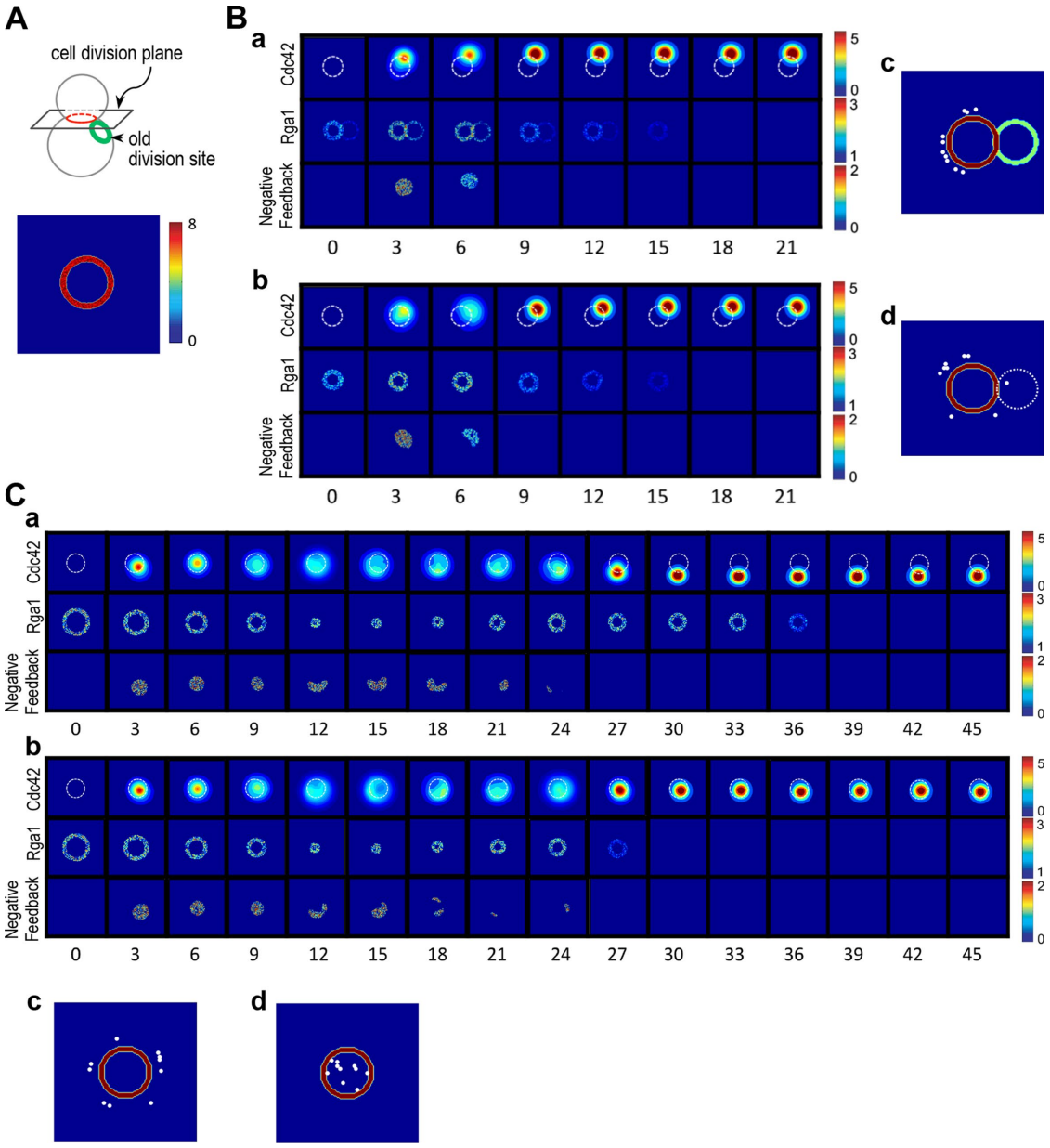

FIGURE 6: Modeling Cdc42 polarization during G1 in *WT* and *rax1*Δ cells. (A) Scheme of an axially budding cell with the current (red ring) and an old cell division site (green ring). The spatial cue distribution (red circle) at the current division site is shown in a two-dimensional computational domain (below). (B) Simulation of Cdc42 polarization with Rga1 distribution at the current and old division site (a and c) or in the absence of Rga1 at an adjacent old bud site (b and d). The first phase with delayed negative feedback is assumed to last for 6 min (t_{off} = 6 min), and Rga1 delocalizes at 18 min, as in mother cells. The white dashed circles with a radius of 0.5 μm are reference positions for the immediately preceding division site. (c, d) White dots mark the positions of the Cdc42-GTP clusters after 21 min from 10 different simulations. (C) Simulation of Cdc42 polarization with transient Rga1 distribution at the current division site and the following assumptions: (a and c) the first phase lasts for 25 min (t_{off} = 25 min), and the Rga1 delocalizes at 39 min; (b, d) the first phase lasts for 25 min (t_{off} = 25 min), and Rga1 delocalizes at 29 min. (c, d) White dots mark the positions of the Cdc42-GTP clusters after 45 min from 10 different simulations.

delocalized during T_1 (Figure 8A), similarly to premature delocalization of GFP-Rga1 in *nba1*Δ cells with minor differences. Local intensity of GFP-Rga1Δm1 at the bud neck and the division site was lower than *WT* GFP-Rga1 prior to cytokinesis, during T_1, and at the T_1/T_2 transition (Figure 8Bb), although the global intensity of both proteins was about the same in large budded cells before cytokinesis (Figure 8Ba). The average duration of T_1 and T_2 in daughter cells was also similar between the strains expressing GFP-Rga1Δm1 and GFP-Rga1 (Figure 8Bc). Since localization of GFP-Rga1Δm1 to the bud neck was reduced prior to cytokinesis (unlike in the case of GFP-Rga1 in *nba1*Δ cells; see Figure 7Bb), the LIM domains may thus affect Rga1's localization even before its interaction with Nba1. Collectively, these observations suggest that Rga1 localizes to the immediately preceding division site via interaction with Nba1 (and likely also with Nis1), similarly to its localization to older division sites (see above).

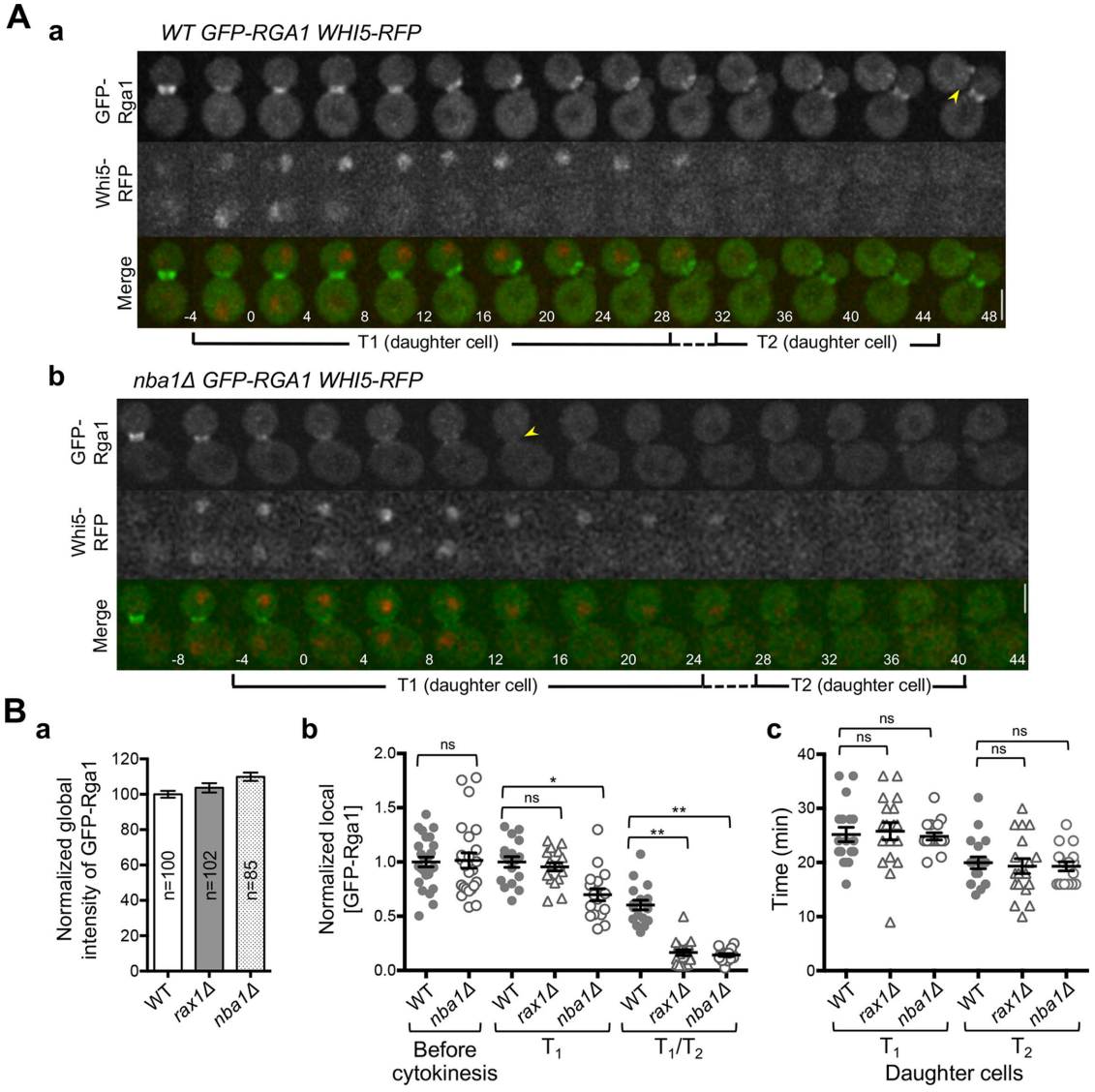

FIGURE 7: Localization of GFP-Rga1 in *WT* and *nba1*Δ cells. (A) Time-lapse images of GFP-Rga1 and Whi5-mCherry in (a) *WT* and (b) *nba1*Δ cells at 30°C. Numbers indicate time (in minutes) from the onset of cytokinesis ($t = 0$). Arrowheads mark when GFP-Rga1 delocalizes (see *Materials and Methods*). Bars, 3 μm. (B) (a) Normalized global intensity (mean ± SEM) of GFP-Rga1 in cells with large buds before cytokinesis. (b) Local intensity of GFP-Rga1 at the bud neck is plotted for individual cells at different cell cycle stages: before cytokinesis (*WT,* $n = 26$; and *nba1*Δ, $n = 24$); peak intensity during T_1; and at the T_1/T_2 transition from time-lapse imaging (*WT,* $n = 17$; *nba1*Δ, $n = 17$; and *rax1*Δ, $n = 18$). Values were normalized to the average GFP-Rga1 intensity prior to cytokinesis in *WT* cells. $^*p = 0.0003$, $^{**}p < 0.0001$; ns, not significant; $p > 0.05$. (c) Length of T_1 and T_2 (min) in each daughter cell (*WT,* $n = 17$; *nba1*Δ, $n = 17$; and *rax1*Δ, $n = 18$). Mean (horizontal lines) ± SEM (error bars).

Premature delocalization of Rga1 in mid G1 may lead to budding within the division site in daughter cells

To explain how the timing of Rga1 delocalization in G1 can affect the orientation of the Cdc42 polarization axis, we extended our computational modeling. When localization of Cdc42 GAP resembled that of Rga1 in *WT* daughter cells (see Figure 6C), our biphasic model for Cdc42 polarization predicted that the Cdc42-GTP cluster level fluctuated around the division site during the first phase and then became stabilized at a single site that is adjacent to the axial landmark (Lee *et al.*, 2015; Figure 6C, a and c). In contrast, when the Cdc42 GAP was assumed to delocalize from the division site prior to the second phase, as in *rax1*Δ or *nba1*Δ daughter cells, Cdc42 always polarized within the division site (Figure 6C, b and d). Therefore, our model recapitulates time-evolved Cdc42 polarization in vivo, consistent with the same site rebudding phenotype of the daughter cells of *rax1*Δ, *rax2*Δ, *nis1*Δ, and *nba1*Δ mutants (see Figure 4A).

Why does this premature delocalization of Rga1 have a more pronounced effect in daughter cells of these mutants? One critical difference between mother and daughter cells is cell size. Since mother cells are larger than newly born daughter cells, the duration of T_1 is shorter (Di Talia *et al.*, 2007). We postulated that this cell-cycle difference could account for the different bud-site selection defect in mother versus daughter cells. To explore this idea, we modeled how different lengths of the first phase (equivalent to T_1) of G1 would affect Cdc42 polarization when premature delocalization of Rga1 was implemented (see Figure 9A). Interestingly, when

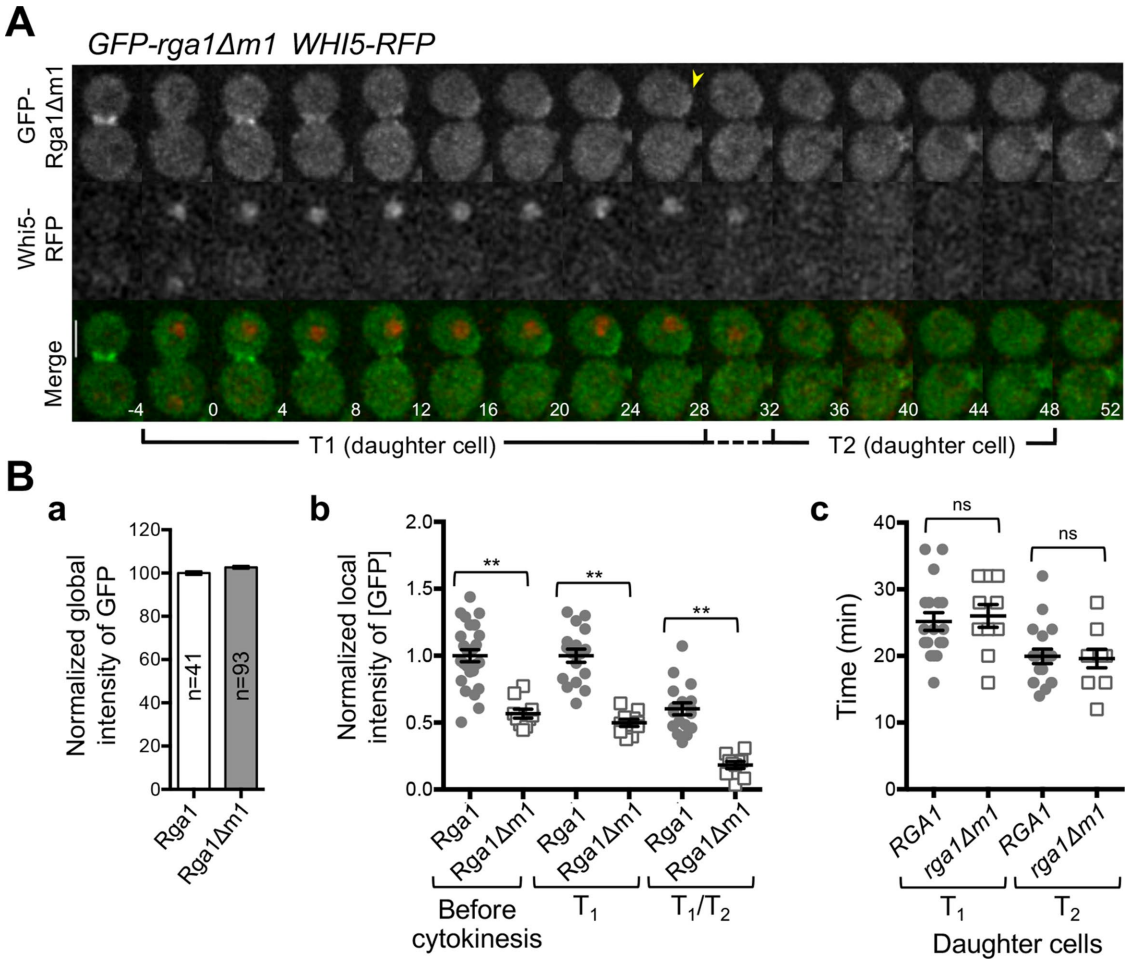

FIGURE 8: Localization of GFP-Rga1Δm1 carrying a deletion of the LIM domains. (A) Localization of GFP-Rga1Δm1 and Whi5-mCherry at 30°C. Numbers indicate time (in min) from the onset of cytokinesis ($t = 0$). An arrowhead marks when GFP-Rga1 delocalizes. Bar, 3 μm. (B) (a) Normalized global intensity (mean ± SEM) of GFP-Rga1 or GFP-Rga1Δm1 in cells with large buds before cytokinesis. (b) Local intensity of GFP-Rga1 or GFP-Rga1Δm1 at the bud neck is shown for individual cells as in Figure 7B. The number of time-lapse images analyzed are as follows: *WT*, $n = 26$ and *GFP-rga1Δm1*, $n = 10$ before cytokinesis, and *WT*, $n = 17$ and *GFP-rga1Δm1*, $n = 10$ at other cell-cycle stages. $^{**}p < 0.0001$; ns, not significant; $p > 0.05$. (c) Length of T_1 and T_2 (min) in each daughter cell (*WT*, $n = 17$; and *GFP-rga1Δm1*, $n = 10$). Mean (horizontal lines) ± SEM (error bars).

the first phase was assumed to last for 10 or 15 min (which is a little longer than T_1 in typical mother cells at 30°C), Cdc42 cluster became stabilized at a site adjacent to the preceding division site (Figure 9, B and C). In contrast, when the first phase was modeled longer than 20 min (T_1 = 25–27 min in daughter cells), Cdc42 repolarized within the division site more frequently in our simulations (Figure 9C). By implementing the similar premature delocalization of Rga1, we ran additional independent simulations with different lengths of the first phase and randomly generated parameters within certain ranges (see *Materials and Methods*). These simulations confirmed that Cdc42 repolarizes within the division site at a higher frequency as the first phase is assumed to last longer (Supplemental Figure S3). Our model thus supports the idea that premature delocalization of Rga1 in the mutants causes a more severe defect in orienting the polarity axis in daughter cells because of their longer T_1 compared with mother cells. An interesting prediction from this model is that even with premature delocalization of Rga1, if a cell traverses G1 rapidly, the cell might be able to establish a proper bud site prior to delocalization of Rga1. To test this prediction by manipulating the G1 length in vivo, we introduced *whi5* deletion into a *rax1*Δ mutant, since cells are smaller and progress through T_1 more quickly in the absence of START inhibitor Whi5 (Jorgensen *et al.*, 2002; Di Talia *et al.*, 2007). We then examined the bud site and birth scar positions of *rax1*Δ *whi5*Δ daughter cells. We found a statistically significant increase of the axial budding events in the *rax1*Δ*whi5*Δ daughter cells compared with *rax1*Δ daughter cells ($^{*}p = 0.01$; Figure 4A). Although *whi5*Δ did not completely rescue the "budding-within-the-birth-scar phenotype" of *rax1*Δ daughters, these observations are consistent with our model's prediction.

DISCUSSION

Despite significant progress made in recent years, how a single axis of cell polarity is established is not fully understood. The axis of Cdc42 polarization in budding yeast is critical for mitotic spindle orientation as well as determination of the plane of cell division. Rga1, a Cdc42 GAP in budding yeast, is required for proper bud-site selection (Stevenson *et al.*, 1995; Chen *et al.*, 1996; Smith *et al.*, 2002; Lo, Lee, *et al.*, 2013) and for preventing rebudding at the previous division site by inhibiting Cdc42 repolarization (Tong *et al.*, 2007). Whether Rga1 functions independently or interacts with

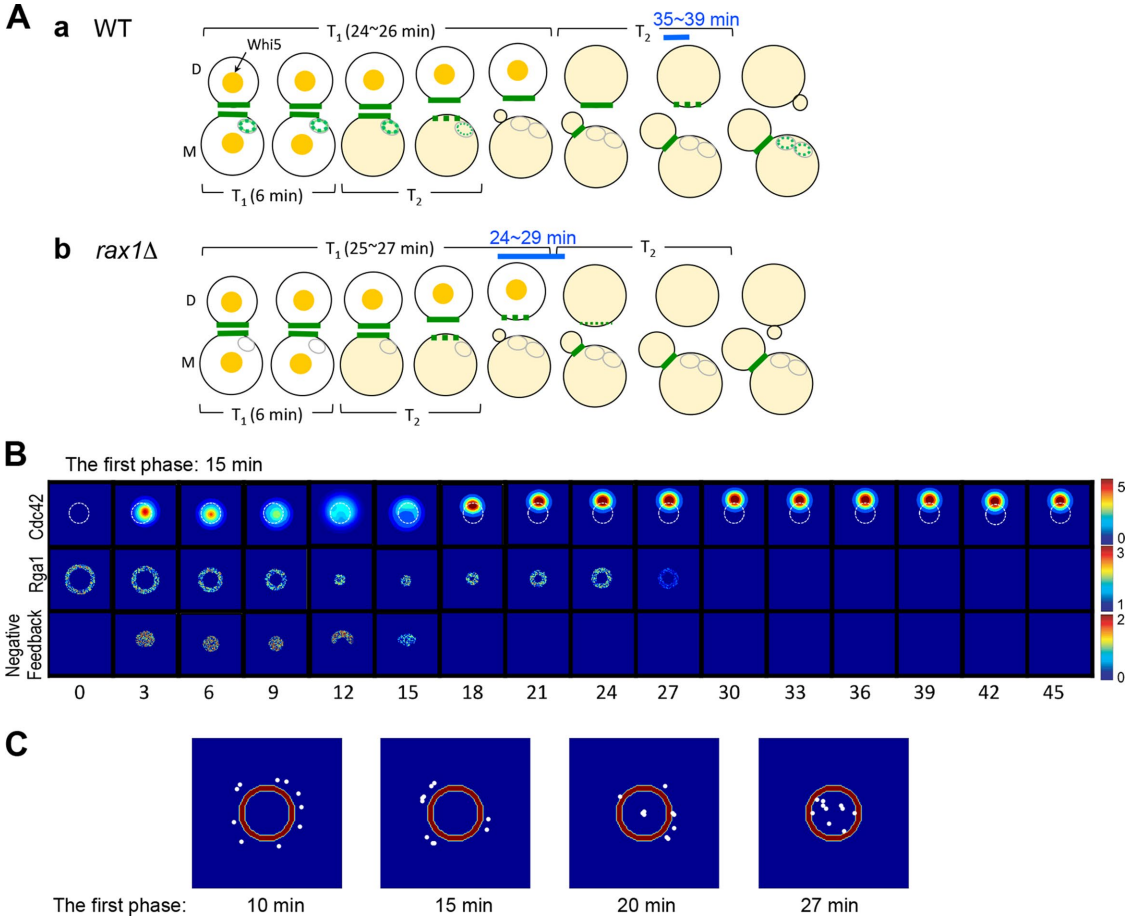

FIGURE 9: Modeling Cdc42 polarization with different lengths of the first phase in mutant haploid daughter cells. (A) Scheme of Rga1 localization (in green) relative to Whi5 (yellow in the nucleus and light yellow in the cytoplasm). Rga1 localizes to the current division site and old bud sites (gray rings) in *WT* (a) but only to the current division site in *rax1*Δ cells (b). Blue bars mark the time window when Rga1 delocalizes in daughter cells. Relative time from the onset of cytokinesis ($t = 0$) at 30°C is marked. (B) Simulation of Cdc42 polarization with time-dependent Rga1 localization and delayed negative feedback in the first phase. The first phase is assumed to last for 15 min ($t_{off} = 15$ min). The Rga1 delocalizes from the division site at 29 min, as in *rax1*Δ daughter cells ($t = 0$ at the onset of cytokinesis). (C) The positions of the Cdc42-GTP clusters at 45 min are shown from 10 independent simulations with the same Rga1 delocalization time (at 29 min) but with different length of the first phase as indicated below. The axial landmark is depicted as a red circle.

other negative polarity cues to prevent Cdc42 repolarization at all previously used divisions sites had been elusive. It was also not clear how Rga1 is recruited to the old division sites. Our studies reported here answer some of these outstanding questions and also raise new ones.

We provide several lines of evidence that Rga1 is recruited to the immediately preceding division site and older division sites by Nba1 and Nis1, which localize to these sites via interaction with Rax1 and Rax2 (Meitinger *et al.*, 2014). However, unlike Nba1, Nis1, Rax1, and Rax2, which are stably anchored to these sites, Rga1 arrives transiently at the old division sites in each cell division cycle. Our FRAP analyses indicate that Rga1 is very dynamic at old division sites as well as at the current division site, unlike Nba1 and Nis1 (Meitinger *et al.*, 2014). It is, however, not known whether and why such transient delivery, as opposed to stable anchoring, of Rga1 to old division sites is necessary. We speculate that a regulatory mechanism might exist to conserve the critical enzyme Rga1 during repeated cell divisions. As expected from their role in recruitment of Rga1 to previous division sites, we find that cells lacking *NBA1*, *NIS1*, *RAX1*, or *RAX2* as well as cells expressing an Rga1 LIM domain mutant protein, which is defective in interaction with Nba1, exhibit improper bud-site selection. While *RAX1* and *RAX2* are known to be involved in bipolar budding of diploid **a**/α cells (Chen *et al.*, 2000; Kang *et al.*, 2004), our analyses of bud scars and birth scar show that haploid *rax1*Δ and *rax2*Δ mutants are also defective in bud-site selection. Because of the relatively minor defect in mother cells of these mutants (see below), the role of Rax1 and Rax2 in axial budding might have been overlooked in previous studies.

We show that Rga1 interacts with Nba1 efficiently in the presence of Zn^{++} ion, consistent with the requirement of Rga1 LIM domains for the interaction. Known functions of LIM domains, which have a characteristic cysteine-rich motif with a zinc-finger structure, include mediating intramolecular and intermolecular protein interactions (Feuerstein *et al.*, 1994; Schmeichel and Beckerle, 1994). The LIM domains might also regulate Rga1 activity, since a Rga1 protein lacking functional LIM domains could suppress defects caused by a mutation of Rho-GAP Bem2 (Chen *et al.*, 1996). In addition, a recent study reported that overexpression of a C-terminal

Rga1 fragment (i.e., lacking the LIM domains) leads to a loss-of-polarity phenotype, while the overexpression of full-length Rga1 results in no defects, suggesting a possible inhibitory function of the N-terminal domain (He *et al.*, 2015). Whether Nba1 is involved only in recruiting Rga1 to previous division sites or also in regulating its GAP activity remains an open question.

We suggest that Rga1 functions in the same pathway with Nba1 and Nis1 to inhibit Cdc42 based on the following data presented in this study: First, localization of Rga1 to the immediately preceding division site as well as older division sites is dependent on Nba1, Nis1, Rax1, and Rax2 (Figures 3 and 7 and Supplemental Figure S2). Second, Rga1 interacts directly with Nba1 and likely with Nis1 (Figure 3). Third, a *rga1*Δ *nba1*Δ double mutant exhibits an almost identical defect of Cdc42 repolarization as *rga1*Δ or *nba1*Δ single mutant (rather than having an additive defect) (Figure 4). Furthermore, an *rga1* mutant lacking LIM domains fails to interact with Nba1 and exhibits a similar defect as *nba1*Δ (Figures 3D, 4, and 8). We note that Meitinger *et al*. (2014) reached a different conclusion from analyses of these mutants. Although we are unsure about the cause of this discrepancy, it is not due to difference of strain backgrounds, since we have examined mutants in two different strain backgrounds including one used in their report (see *Materials and Methods*). Our analyses distinguished the cell division sites in mother and daughter cells by staining with two fluorescent dyes, while their analyses did not separate mother and daughter cells but used transmission electron microscopy images to visualize a bud-neck "collar" (excess cell wall material indicative of rebudding at a previously used site). We speculate that the previous study might have reached a similar conclusion about the functional interaction between Rga1 and Nba1-Nis1, if it had included separate analyses of daughter cells in addition to the cytokinesis remnants remained at the old division sites in mother cells. To clarify this issue will require further investigation.

It has been suggested that Nba1 and Nis1 prevent Cdc42 reactivation at previous division sites by inhibiting the interaction between the Cdc24 polarity complex and Rsr1 (Meitinger *et al.*, 2014). While we cannot rule out the possibility that another mechanism may also be involved in the process, we favor the idea that the inhibitory function of Nba1 in Cdc42 repolarization at the old division sites relies on the recruitment of Rga1. We thus propose inhibitory pathways for Cdc42 polarization as follows (Figure 10): During cytokinesis, Rga1 and Gps1-Nba1-Nis1 inhibit Cdc42 polarization at the current division site (Tong *et al.*, 2007; Meitinger *et al*. 2013). Once cytokinesis and septation have been completed, that is, when Rax1-Rax2 have arrived at the immediately preceding division site (Kang *et al.*, 2004), Nba1 and Nis1 are anchored to the site via interaction with Rax1-Rax2 (Meitinger *et al.*, 2014). This complex at the immediately preceding division site then recruits Rga1, which inhibits Cdc42 (this study). Rga1 is also recruited to older division sites and inhibits Cdc42 repolarization, although Rga1's role at the old division site(s) seems to be relatively less critical (this study). Similarly, Meitinger *et al*. (2014) noted that disruption of Nba1 at the immediately preceding division site (referred to as "emergent CRMs") caused a greater defect in Cdc42 inhibition than removal of Nba1 from older cell division sites. How these protein–protein interactions are altered during cytokinesis and subsequent G1 also remains an open question.

An unexpected, interesting finding from this study is the distinct effect of Rga1 distribution on polarization of mother versus daughter cells. While Rga1 localization to the immediately preceding division site is critical for positioning a proper bud site in daughter cells, this localization has a relatively minor role in mother cells. This is likely due to the intrinsic difference in the cell-cycle progression (Di Talia *et al.*, 2007). Selection of a bud site and thus establishing the axis of Cdc42 polarization occur long after cytokinesis in daughter cells, unlike in mother cells (Lee *et al.*, 2015). Consequently, Rga1 localization to the current division site is most critical in mother cells (Tong *et al.*, 2007), whereas transient localization of Rga1 to both current division site and immediately preceding division site until T_1/T_2 transition are equally important in daughter cells (this study). Indeed, our mathematical modeling can recapitulate distinct dynamics of Cdc42 polarization in mother and daughter cells by implementing transient distribution of Cdc42 GAP (Lee *et al.*, 2015; this study). According to our model, Cdc42 is more likely to repolarize within the previous division site when the first temporal phase of G1 is longer and premature delocalization of Cdc42 GAP is implemented (as observed in *rax1*Δ or *nba1*Δ mutants). This model thus provides a possible explanation for the different phenotypes of the mutant mother and daughter cells. A logical extension of this model is that even with premature delocalization of Rga1 from the division site, if a cell is forced to pass through T_1 rapidly, then the cell might be able to establish a proper bud site. Our experimental test of this

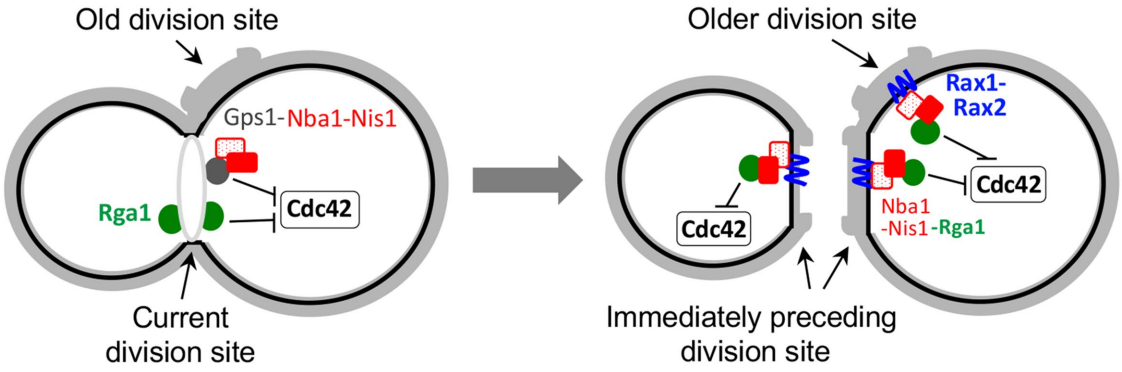

FIGURE 10: Model for inhibition of Cdc42 repolarization at the current and old cell division sites. During cytokinesis, Rga1 (green circle) and the Nba1-Nis1-Gps1 inhibit Cdc42 repolarization to the division site. After cytokinesis and septum formation, Nba1-Nis1 (solid and dotted red boxes) are inherited to the immediately preceding site and remain at the older division sites via interaction with Rax1/Rax2 (blue lines). Rga1 is recruited to the immediately preceding site as well as at the older division sites via interaction with Nba1-Nis1. Rga1 then inhibits Cdc42 repolarizaiton at these previous cell division sites. The complex at the old division site is omitted in the cell shown on the left.

prediction by introducing a *whi5* deletion to shorten G1 resulted in only partial rescue of the *rax1*Δ daughter cells. A caveat to such a test is that deleting the key START regulator Whi5 might affect not only T_1 length but also potentially the activity or assembly of the polarity complex. Because cell-to-cell variations of the G1 length is observed even in *WT* cells (Di Talia *et al.*, 2007), it would also be imperative to access the G1 length of individual cells and examine its correlation with the budding pattern. Other factors at the division sites might also contribute to differential Cdc42 polarization in mother versus daughter cells of these mutants. For example, distinct components in bud scar versus birth scar might affect these cortical polarity components differently. While a crucial test waits for a deeper understanding of regulation of these polarity factors, our modeling introduces an intriguing concept that delicate coordination of the spatial distribution of a Cdc42 GAP with cell-cycle progression is critical for establishing a proper axis of cell polarization and thus selection of a new nonoverlapping plane of cell division in budding yeast.

MATERIALS AND METHODS

Strains, plasmids, and general methods

Standard methods of yeast genetics, DNA manipulation, and growth conditions were used (Guthrie and Fink, 1991). All yeast strains used for imaging express tagged and truncated genes under their native promoters from the chromosomes. Yeast strains and plasmids used in this study are listed in Supplemental Tables S1 and S2, respectively, with a brief description of construction methods.

Microscopy and image analysis

Cells were grown in appropriate synthetic medium overnight and then freshly subcultured for 3–4 h in the same medium. Time-lapse imaging was performed at 30°C (except those indicated, at 22°C) essentially as previously described (Kang *et al.*, 2014) using a spinning disk confocal microscope (Ultra-VIEW VoX CSU-X1 system; Perkin Elmer-Cetus) equipped with a 100×; 1.4 NA Plan Apochromat objective lens (Nikon); 440-, 488-, 515- and 561-nm solid-state lasers (Modular Laser System 2.0; Perkin Elmer-Cetus); and a back-thinned electron-multiplying charge-coupled device (CCD) camera (ImagEM C9100-13; Hamamatsu Photonics) on an inverted microscope (Ti-E; Nikon). For most time-lapse imaging, images were captured (9 z-stacks; 0.3 µm step) every 2 or 4 min using cells either mounted on an agarose slab or in a glass-bottomed dish (MatTek) containing medium with 5 µM propyl gallate (Sigma), an anti-fade reagent. Cells were adhered onto the microwell of the dish, which was pretreated with 0.2% concanavalin A (Sigma) and then covered with proper medium containing 0.6% agarose and propyl gallate. For long-term time-lapse microscopy (in Figure 2A), images were captured every 6 min at 30°C. For Figure 1B, time-lapse images were captured (11 z-stacks; 0.4 µm step, 4-min interval) after staining cells with Calcofluor White (see below).

SIM was performed using a GE DeltaVision OMX SR equipped with an Olympus 60× (1.42 NA) objective lens. Static images were captured (19 z-stacks; 0.125 µm step) at 25°C. Cells were mounted onto a glass-bottomed dish as described above. SoftwoRx v6.5.2 was used to capture images and create three-dimensional projections.

Image processing and analyses were performed using ImageJ (National Institutes of Health). Maximum intensity projections of z-stacks were generated to make figures and videos, except where noted. To estimate colocalization, z-stack images were used after background subtraction to calculate Pearson's correlation coeffcient (PCC) using the Coloc 2 plug-in, and PCC >0.5 was considered as colocalization.

To quantify the local fluorescence intensity of GFP-Rga1, first a rectangular region of interest (ROI) that included the GFP-Rga1 signal was used to measure the intensity from z-stacks. A second ROI that included the first ROI and the surrounding cytoplasmic region (approximately twice as big as the first ROI) was used for background subtraction (Coffman *et al.*, 2011). The intensity of GFP-Rga1 at the bud neck before cytokinesis (i.e., 3 min before the Cdc3-mCherry ring split), peak intensity of GFP-Rga1 localized at the division site during T_1, and GFP-Rga1 localized to the division site at the T_1/T_2 transition were measured for each individual cell. For global intensity quantification, average intensity projections were created from all 9 z-sections at 0.3 µm spacing, and an ROI was drawn around the outline of cells. The intensity of *WT* cells without any fluorescently tagged proteins were used to subtract background. To determine the time when GFP-Rga1 delocalized from the immediately preceding division site in daughter cells (marked with a yellow arrowhead in Figures 7 and 8 and Supplemental S2A), the same threshold was applied to quantify the GFP-Rga1 intensity at each time point using ImageJ.

To quantify the Whi5-mCherry signal in the nucleus at each time point, a circular ROI that included the Whi5-mCherry signal in the nucleus was used to measure the intensity from z-stack images. Background subtraction was done as described above for GFP-Rga1. The duration time of T_1 and T_2 was determined by monitoring the intensity of the nuclear Whi5-mCherry signal as well as the onset of cytokinesis (identified by a split Cdc3-mCherry ring) and bud emergence in individual mother and daughter cells. The T_1/T_2 transition was marked when the Whi5-mCherry intensity in the nucleus was ~50% of its peak level. The duration time of T_1 and T_2 was found to be similar for all the strains examined in this study (ns: $p > 0.6$; Figures 7Bc and 8Bc).

Kymographs and heatmaps were generated from maximum intensity projection images of z-stacks, except noted, using the multiple kymograph plug-in and heat map histogram plug-in for ImageJ. Kymograph of Cdc3-GFP, in Supplemental Figure S2Bb, was generated from a single z-stack to show the hollow septin ring more clearly.

FRAP analysis

Images were captured at a single z-section on a gelatin slab at 22°C using the photokinesis unit on the Ultra-VIEW VoX confocal system (see above), similarly to the assays described previously (Coffman *et al.*, 2009). Prior to beginning each FRAP experiment, a z-stack image was taken with the 561-nm laser to examine Cdc3-mCherry signal and select cells in specific stages of the cell cycle. In the FRAP assay, the middle focal plane of cells was bleached to <50% of the original fluorescence intensity after collecting five prebleach images. Postbleach images were acquired for a duration long enough such that the recovery curve reached a plateau. Background and photobleaching during image acquisition were corrected using empty space among cells and unbleached cells in the same image. The prebleach intensity of the ROI was normalized to 100%, and the first postbleach intensity was normalized to 0%. The intensities of every three consecutive postbleach time points were averaged to reduce noise. Then the intensity data were plotted and fitted using the exponential decay equation $y = m_1+m_2 \exp(-m_3x)$, where m_3 is the off-rate, using Prism 6 (GraphPad Software). The half-time of recovery was calculated using the equation $t_{1/2} = \ln 2/m_3$.

Analysis of cell division sites

Bud scars and birth scars were stained with Calcofluor White (0.5 µg/ml) and WGA-FITC (100 µg/ml), as previously described

(Lee *et al.*, 2015). Maximum intensity projections were generated from 17 z-stacks (0.3 μm step size) of images captured with a fluorescence microscope (E800; Nikon) fitted with a 100× 1.3NA oil Plan Fluor objective lens (Nikon), a CCD camera (ORCA-ER; Hamamatsu Photonics), and FITC-GFP and DAPI (4′,6-diamidino-2-phenylindole) filters (Intelligent Imaging Innovations). Cell division sites were analyzed in three independent experiments. The budding pattern of *ESM356-1 nba1*Δ cells was determined from time-lapse images by analyzing the position of the new septin ring in relation to the old septin ring (marked with Cdc3-mCherry). We found that the majority of mother cells appeared to bud in an axial pattern (84%, $n = 32$), similarly to *nba1*Δ mutants in the YEF473A (Bi and Pringle, 1996) strain background. Staining of both bud scars and birth scar indicated that the bud scars were adjacent to one another but within the birth scar in the majority of mother cells of this mutant (see the text and Figure 4).

Yeast two-hybrid assay

Two-hybrid assays were performed using EGY48 carrying the *LEU2* reporter (and the *lacZ* reporter plasmid pSH18-34, *URA3*), as previously described (Gyuris *et al.*, 1993). The full-length, N-terminal half (amino acids 1–537) and the C-terminal half (amino acids 538–1007) of Rga1 were expressed as DNA-binding domain fusions using pEG202 clones (Supplemental Table S2). The full-length Nba1 and Nis1 were expressed as activation domain fusions using pJG4-5 clones (Supplemental Table S2). pJG4-5-cdc42^{G12V} (a gift from M. Peter, ETH Zurich, Switzerland) carries the C188S mutation (in addition to G12V) to avoid membrane targeting (Butty *et al.*, 2002). About 1.5×10^5 cells of each transformant of a DBD and an AD fusion or a vector control were spotted on SGal-His-Trp-Ura and SGal-His-Trp-Ura-Leu plates and incubated at 30°C for 4–5 d. At least three independent transformants of a DBD and an AD fusion were tested and spot assays were repeated in triplicate.

In vitro binding assay and immunoblotting

GST or MBP fusion proteins were expressed in protease-deficient *E. coli* cells (BL21-CodonPlus), and in vitro binding assays were performed using the S10 fraction as previously described (Kozminski *et al.*, 2003; Kang *et al.*, 2014) except some modifications described below. Cell lysates carrying MBP fusion proteins were prepared using a lysis buffer (10 mM sodium phosphate buffer, pH 8.0, 500 mM NaCl, 10 mM β-mercaptoethanol, 1 mM EGTA (ethylene glycol-bis(β-aminoethyl ether)-*N*,*N*,*N*′,*N*′-tetraacetic acid), 0.2% Triton X-100). To pull down MBP fusion proteins, the S10 fraction was incubated with 40 μl amylose resin (New England BioLabs) for 1 h at 4°C by rocking. The beads were then washed four times using the same lysis buffer and once using a binding buffer (10 mM sodium phosphate buffer [pH 8.0], 100 mM NaCl, 10 mM β-mercaptoethanol, 0.2% Triton X-100, 50 μM $Zn(OAc)_2$) or the same buffer without $Zn(OAc)_2$. The S10 fractions containing GST-Rga1^N or GST-Rga1$^{N\Delta m1}$ were prepared using the same binding buffer with or without 50 μM $Zn(OAc)_2$. To perform binding assays, the S10 fractions containing GST-Rga1^N and GST-Rga1$^{N\Delta m1}$ were incubated with an equal amount of MBP-Nba1 (or MBP-Nis1 or MBP control) on amylose resin either in the presence or absence of Zn^{++} for 2.5 h at 4°C by rocking. After washing the amylose resin using the binding buffer with or without Zn^{++} (see above), proteins were eluted from the resin with Laemmli sample buffer and subjected to SDS–PAGE and immunoblotting. GST- and MBP-fusion proteins were detected using monoclonal antibodies against GST (Novus Biologicals) and polyclonal rabbit anti-MBP antibodies (New England Biolabs), respectively. Protein bands were then visualized using Alexa Fluor 680 goat anti-rabbit immunoglobulin G (IgG; Molecular Probes) or IRDye 800CW-conjugated goat anti-mouse IgG (LI-COR Biosciences) secondary antibodies and the Odyssey CLx system (LI-COR Biosciences). Proteins were quantified using the software of the Odyssey CLx system, and relative recovery of GST-Rga1^N or GST- Rga1$^{N\Delta m1}$ was estimated by the ratio of each pulled-down protein over the input and then normalized against pulled-down MBP fusion proteins. Binding assays were repeated two to four times with or without Zn^{2+} for each combination of proteins, and the average recovery was calculated (see legend to Figure 3D).

Statistical analysis

Data analysis was performed using Prism 6 (GraphPad Software). A two-tailed Student's *t* test was performed to determine statistical differences between two sets of data.

MODELING

A two-dimensional model of Cdc42

A two-dimensional model applied in the study is based on our previous model, and the details are previously described (Lee *et al.*, 2015). Briefly, the model consists of the particle density of membrane-bound Cdc42, denoted by *a*. The computational domain, denoted by *M* in the model, is a two-dimensional region of cell membrane, in which the landmark cue is located at the center. For simplicity, we assume that membrane-bound Cdc42 appears only in this domain and the domain is taken as planar without considering the effect of the surface curvature. Another key assumption is mass conservation: that is, the total number of molecules in the whole cell remains constant in time (Altschuler *et al.*, 2008; Howell *et al.*, 2009; Lo, Lee, *et al.*, 2013).

The dynamics of *a* is governed by the following reaction-diffusion equation:

$$\frac{\partial a}{\partial t} = D_m \Delta a + F\big(a(x,t), u(x,t)\big)\big(1-\phi(a)\big) - k_{\text{off}}\big(a\big(x, t-t_1\big), x, t\big)a$$

with the function $\phi(a)$ defined as the average value of *a* over the membrane, namely, $\hat{a} = \int_M a\,dx / |M|$ (Lo, Lee, *et al.*, 2013; Lo *et al.*, 2014), where $|M|$ equals the total area of domain *M*. Three key components of Cdc42 dynamics included in the model are lateral membrane diffusion of Cdc42, recruitment (activation) of Cdc42 from the cytoplasm to the membrane, and the reverse reaction (Altschuler *et al.*, 2008).

The activation term is based on the following form of feedback:

$$F\big(a(x,t), u(x)\big) = \theta_1(t)\left(u(x) + k_{\text{on1}}\frac{\big(a(x,t)/K_1\big)^2}{1+\phi\Big(\big(a(x,t)/K_1\big)^2\Big)}\right) + k_{\text{on2}}\big(1-\theta_1(t)\big)\frac{\big(a(x,t)/K_2\big)^2}{1+\phi\Big(\big(a(x,t)/K_2\big)^2\Big)}$$

In the formula, the first term of the right-hand side represents the axial landmark [denoted by $u(x)$] and the Rsr1 module feedback (Goryachev and Pokhilko, 2008; Howell *et al.*, 2009; Lo, Lee, *et al.*, 2013; Lo *et al.*, 2014; Goryachev and Leda, 2017), with K_1 a normalizing factor; the second term of the right-hand side represents the feedback in Cdc42-signaling network. We consider two temporal phases: 1) in the first phase, the axial landmark and the Rsr1 module are involved in positive feedback; 2) in the second phase, the spatial cue is excluded and the Cdc42-signaling feedback is active with

stronger positive feedback strength. Since we assume that the feedback is stronger than the Rsr1 module feedback, we apply smaller normalizing factor K_2 ($<K_1$) here.

The function is defined as

$$u(x) = \delta_u(x) Ri(x),$$

where $\delta_u(x)$ is a spatial uncorrelated random function with uniform distribution between 0 and 1 for each x; $Ri(x)$ is defined as

$$\begin{cases} Ri(x) = 8 \text{ if } 0.6 \le |x| \le 0.75 \\ Ri(x) = 0 \text{ otherwise} \end{cases}$$

The on–off function $\theta_1(t)$ controls a switch from time phase 1 and time phase 2 at time t_{off}, and $\theta_1(t)$ is defined as

$$\theta_1(t) = \frac{e^{(t_{off}-t)/\varepsilon}}{1+e^{(t_{off}-t)/\varepsilon}}$$

where ε is a very small value $(\varepsilon = 0.01)$.

Similarly to the activation term, we define the deactivation term as

$$k_{off}(a(x, t-t_1), x, t) = g(x,t) + 3\theta_1(t)\delta_d(x)H(a(x,t-t_1) - K_{off})$$

where H is defined as

$$\begin{cases} H(a) = 0 \text{ if } a \le 0 \\ H(a) = 1 \text{ if } a > 0 \end{cases}$$

The function $g(x,t)$ will be specified later in "parameter settings." Note that the negative feedback functions when $a(x, t–t_1)$ is larger than K_{off}. $\delta_d(x,t)$ is a spatiotemporal uncorrelated random function with uniform distribution between 0 and 1 for each x and t.

Parameter settings

Based on previous studies (Goryachev and Pokhilko, 2008; Lo, Lee, *et al.*, 2013), the diffusion rate of Cdc42 on the membrane was around 0.1–0.15 μm^2 min^{-1}; the recruitment rate and the activation rate of Cdc42 were 10 and 0.1 min^{-1}, respectively; the normalizing parameter K_1 was taken to be less than 0.3 to achieve spontaneous budding without spatial cues. In this paper, we take D_m = 0.1 μm^2 min^{-1}; and since the activation/recruitment process considered here combines both activation and recruitment processes, we take k_{on1} = k_{on2} = 1 min^{-1}, K_1 = 0.3, and K_2 = 0.2. We take K_2 less than K_1, because we assume that the second feedback is stronger than the first one. Based on our previous work (Lee *et al.*, 2015), we take the parameters for modeling delayed negative feedback as K_{off} = 2, the threshold of Cdc42 for functioning negative feedback; and t_1 = 1 min, the time delay for negative feedback. For modeling the change of Rga1 distribution, we define the function $g(x,t)$ according to the changes of the nonzero regions (higher value = 3, lower value = 1, r is the distance from a point to the center of the domain, r' is the distance from a point to the point 1 μm right to the center of the domain):

1. For wild-type daughter cells, we take {0.35(1 – t/10) + 0.35 < r < 0.35(1 – t/10) + 0.65} for 0 < t < 10; {r < 0.35} for 10 < t < 15; {0.35(t – 15)/8 < r < 0.35(t – 15)/8 + 0.3} for 15 < t < 23; {0.35 < r < 0.65} for 23 < t < 32.2. The Rga1 ring level is decreasing at 32.2 min and totally delocalizes at 39 min in WT daughter cells.
2. For wild-type mother cells, we take {0.3 < r < 0.65} for 0 < t < 3; {0.3 < r < 0.65}; {0.5 < r' < 0.65} for 3 < t < 6. The Rga1 ring level is decreasing at 6 min and totally delocalizes at 18 min in WT mother cells.

The parameter t_{off} depends on the time the first phase ends in different types of cells and mutations, and the values are mentioned in each figure legend.

For each simulation in Supplemental Figure S3, we generate three independent random variables (δ_1, δ_2, and δ_3) from a uniform distribution between 0.5 and 1.5 and then set k_{on1} = k_{on2} = δ_1, the highest value of the function $g(x,t) = 3\delta_2$, $K_1 = 0.3\delta_3$, and $K_2 = 0.2\delta_3$.

ACKNOWLEDGMENTS

We thank C. S. Chan, G. Pereira, S. Martin, E. Bi, M. Peter, J.-Q. Wu, and B. Andrews for plasmids and strains; Y. Zhu and J.-Q. Wu for technical help; S. Cole and A. Jablonski for access to GE DeltaVision OMX SR; and A. Hopper for comments on the manuscript. This work was supported by a research grant (R01 GM114582) from the National Institutes of Health/National Institute of General Medical Sciences to H-O. P. and a CityU Strategic Research Grant (Project No. 7004697) and a general research fund from the Research Grants Council of Hong Kong (Project No. 11303117) to W.C.L.

REFERENCES

Boldface names denote co–first authors.

Altschuler SJ, Angenent SB, Wang Y, Wu LF (2008). On the spontaneous emergence of cell polarity. Nature 454, 886–889.

Bacon JD, Davidson ED, Jones D, Taylor I F (1966). The location of chitin in the yeast cell wall. Biochem J 101, 36c–38c.

Barton AA (1950). Some aspects of cell division in *Saccharomyces cerevisiae*. J Gen Microbiol 4, 84–86.

Bender A, Pringle JR (1989). Multicopy suppression of the *cdc24* budding defect in yeast by *CDC42* and three newly identified genes including the ras-related gene *RSR1*. Proc Natl Acad Sci USA 86, 9976–9980.

Bi E, Park H-O (2012). Cell polarization and cytokinesis in budding yeast. Genetics 191, 347–387.

Bi E, Pringle JR (1996). ZDS1 and ZDS2, genes whose products may regulate Cdc42p in *Saccharomyces cerevisiae*. Mol Cell Biol 16, 5264–5275.

Butty A-C, Perrinjaquet N, Petit A, Jaquenoud M, Segall JE, Hofmann K, Zwahlen C, Peter M (2002). A positive feedback loop stabilizes the guanine-nucleotide exchange factor Cdc24 at sites of polarization. EMBO J 21, 1565–1576.

Cabib E, Bowers B (1971). Chitin and yeast budding: localization of chitin in yeast bud scars. J Biol Chem 246, 152–259.

Caviston JP, Longtine M, Pringle JR, Bi E (2003). The role of Cdc42p GTPase-activating proteins in assembly of the septin ring in yeast. Mol Biol Cell 14, 4051–4066.

Chant J, Corrado K, Pringle JR, Herskowitz I (1991). Yeast *BUD5*, encoding a putative GDP-GTP exchange factor, is necessary for bud site selection and interacts with bud formation gene *BEM1*. Cell 65, 1213–1224.

Chant J, Herskowitz I (1991). Genetic control of bud site selection in yeast by a set of gene products that constitute a morphogenetic pathway. Cell 65, 1203–1212.

Chant J, Pringle JR (1995). Patterns of bud-site selection in the yeast *Saccharomyces cerevisiae*. J Cell Biol 129, 751–765.

Chen GC, Zheng L, Chan CS (1996). The LIM domain-containing Dbm1 GTPase-activating protein is required for normal cellular morphogenesis in *Saccharomyces cerevisiae*. Mol Cell Biol 16, 1376–1390.

Chen T, Hiroko T, Chaudhuri A, Inose F, Lord M, Tanaka S, Chant J, Fujita A (2000). Multigenerational cortical inheritance of the Rax2 protein in orienting polarity and division in yeast. Science 290, 1975–1978.

Coffman VC, Nile AH, Lee I-J, Liu H, Wu J-Q (2009). Roles of formin nodes and myosin motor activity in Mid1p-dependent contractile-ring assembly during fission yeast cytokinesis. Mol Biol Cell 20, 5195–5210.

Coffman VC, Wu P, Parthun MR, Wu J-Q (2011). CENP-A exceeds microtubule attachment sites in centromere clusters of both budding and fission yeast. J Cell Biol 195, 563–572.

Di Talia S, Skotheim JM, Bean JM, Siggia ED, Cross FR (2007). The effects of molecular noise and size control on variability in the budding yeast cell cycle. Nature 448, 947–951.
Drubin DG, Nelson WJ (1996). Origins of cell polarity. Cell 84, 335–344.
Etienne-Manneville S (2004). Cdc42—the centre of polarity. J Cell Sci 117, 1291–1300.
Feuerstein R, Wang X, Song D, Cooke NE, Liebhaber SA (1994). The LIM/double zinc-finger motif functions as a protein dimerization domain. Proc Natl Acad Sci USA 91, 10655–10659.
Freifelder D (1960). Bud position in *Saccharomyces cerevisiae*. J Bacteriol 80, 567–568.
Goryachev AB, Leda M (2017). Many roads to symmetry breaking: molecular mechanisms and theoretical models of yeast cell polarity. Mol Biol Cell 28, 370–380.
Goryachev AB, Pokhilko AV (2008). Dynamics of Cdc42 network embodies a Turing-type mechanism of yeast cell polarity. FEBS Lett 582, 1437–1443.
Guthrie C, Fink GR (1991). Guide to Yeast Genetics and Molecular Biology, San Diego, CA: Academic Press, 194.
Gyuris J, Golemis E, Chertkov H, Brent R (1993). Cdi1, a human G1 and S phase protein phosphatase that associates with Cdk2. Cell 75, 791–803.
He F, Nie WC, Tong Z, Yuan SM, Gong T, Liao Y, Bi E, Gao XD (2015). The GTPase-activating protein Rga1 interacts with Rho3 GTPase and may regulate its function in polarized growth in budding yeast. PLoS One 10, e0123326.
Hicks JB, Strathern JN, Herskowitz I (1977). Interconversion of yeast mating types III. Action of the homothallism (*HO*) gene in cells homozygous for the mating type locus. Genetics 85, 395–405.
Howell AS, Savage NS, Johnson SA, Bose I, Wagner AW, Zyla TR, Nijhout HF, Reed MC, Goryachev AB, Lew DJ (2009). Singularity in polarization: rewiring yeast cells to make two buds. Cell 139, 731–743.
Johnson DI (1999). Cdc42: an essential Rho-type GTPase controlling eukaryotic cell polarity. Microbiol Mol Biol Rev 63, 54–105.
Johnson DI, Pringle JR (1990). Molecular characterization of CDC42, a Saccharomyces cerevisiae gene involved in the development of cell polarity. J Cell Biol 111, 143–152.
Jorgensen P, Nishikawa JL, Breitkreutz BJ, Tyers M (2002). Systematic identification of pathways that couple cell growth and division in yeast. Science 297, 395–400.
Kadrmas JL, Beckerle MC (2004). The LIM domain: from the cytoskeleton to the nucleus. Nat Rev Mol Cell Bio 5, 920–931.
Kang PJ, Angerman E, Jung CH, Park H-O (2012). Bud4 mediates the cell-type-specific assembly of the axial landmark in budding yeast. J Cell Sci 125, 3840–3849.
Kang PJ, Angerman E, Nakashima K, Pringle JR, Park H-O (2004). Interactions among Rax1p, Rax2p, Bud8p, and Bud9p in marking cortical sites for bipolar bud-site selection in yeast. Mol Biol Cell 15, 5145–5157.
Kang PJ, Beven L, Hariharan S, Park H-O (2010). The Rsr1/Bud1 GTPase interacts with itself and the Cdc42 GTPase during bud-site selection and polarity establishment in budding yeast. Mol Biol Cell 21, 3007–3016.
Kang PJ, Lee ME, Park H-O (2014). Bud3 activates Cdc42 to establish a proper growth site in budding yeast. J Cell Biol 206, 19–28.
Kang PJ, Sanson A, Lee B, Park H-O (2001). A GDP/GTP exchange factor involved in linking a spatial landmark to cell polarity. Science 292, 1376–1378.
Khmelinskii A, Keller PJ, Bartosik AA, Meurer M, Barry JD, Mardin BR, Kaufmann A, Trautmann S, Wachsmuth M, Pereira G, *et al*. (2012). Tandem fluorescent protein timers for *in vivo* analysis of protein dynamics. Nat Biotechnol 30, 708–714.
Kim HB, Haarer BK, Pringle JR (1991). Cellular morphogenesis in the Saccharomyces cerevisiae cell cycle: localization of the CDC3 gene product and the timing of events at the budding site. J Cell Biol 112, 535–544.
Kozminski KG, Beven L, Angerman E, Tong AH, Boone C, Park H-O (2003). Interaction between a Ras and a Rho GTPase couples selection of a growth site to the development of cell polarity in yeast. Mol Biol Cell 14, 4958–4970.
Lee ME, Lo W-C, Miller KE, Chou C-S, Park H-O (2015). Regulation of Cdc42 polarization by the Rsr1 GTPase and Rga1, a Cdc42 GTPase-activating protein, in budding yeast. J Cell Sci 128, 2106–2117.
Lippincott J, Shannon KB, Shou W, Deshaies RJ, Li R (2001). The Tem1 small GTPase controls actomyosin and septin dynamics during cytokinesis. J Cell Sci 114, 1379–1386.
Lo W-C, Lee ME, Narayan M, Chou C-S, Park H-O (2013). Polarization of diploid daughter cells directed by spatial cues and GTP hydrolysis of Cdc42 in budding yeast. PLoS One 8, e56665.
Lo W-C, Park H-O, Chou CS (2014). Mathematical analysis of spontaneous emergence of cell polarity. Bull Math Biol 76, 1835–1865.
Meitinger F, Khmelinskii A, Morlot S, Kurtulmus B, Palani S, Andres-Pons A, Hub B, Knop M, Charvin G, Pereira G (2014). A memory system of negative polarity cues prevents replicative aging. Cell 159, 1056–1069.
Meitinger F, Richter H, Heisel S, Hub B, Seufert W, Pereira G (2013). A safeguard mechanism regulates Rho GTPases to coordinate cytokinesis with the establishment of cell polarity. PLoS Biol 11, e1001495.
Miller PJ, Johnson DI (1997). Characterization of the Saccharomyces cerevisiae cdc42-1ts allele and new temperature-conditional-lethal cdc42 alleles. Yeast 13, 561.
Mortimer RK, Johnston JR (1959). Life span of individual yeast cells. Nature 183, 1751–1752.
Nelson WJ (2003). Adaptation of core mechanisms to generate cell polarity. Nature 422, 766–774.
Oh Y, Bi E (2011). Septin structure and function in yeast and beyond. Trends Cell Biol 21, 141–148.
Okada S, Leda M, Hanna J, Savage NS, Bi E, Goryachev AB (2013). Daughter cell identity emerges from the interplay of Cdc42, septins, and exocytosis. Dev Cell 26, 148–161.
Okada S, Lee ME, Bi E, Park H-O (2017). Probing Cdc42 polarization dynamics in budding yeast using a biosensor. Methods Enzymol 589, 171–190.
Ozbudak EM, Becskei A, van Oudenaarden A (2005). A system of counteracting feedback loops regulates Cdc42p activity during spontaneous cell polarization. Dev Cell 9, 565–571.
Park H-O, Bi E (2007). Central roles of small GTPases in the development of cell polarity in yeast and beyond. Microbiol Mol Biol Rev 71, 48–96.
Park H-O, Bi E, Pringle JR, Herskowitz I (1997). Two active states of the Ras-related Bud1/Rsr1 protein bind to different effectors to determine yeast cell polarity. Proc Natl Acad Sci USA 94, 4463–4468.
Park H-O, Chant J, Herskowitz I (1993). *BUD2* encodes a GTPase-activating protein for Bud1/Rsr1 necessary for proper bud-site selection in yeast. Nature 365, 269–274.
Richman TJ, Sawyer MM, Johnson DI (2002). *Saccharomyces cerevisiae* Cdc42p localizes to cellular membranes and clusters at sites of polarized growth. Eukaryot Cell 1, 458–468.
Schmeichel KL, Beckerle MC (1994). The LIM domain is a modular protein-binding interface. Cell 79, 211–219.
Smith GR, Givan SA, Cullen P, Sprague GF Jr (2002). GTPase-activating proteins for Cdc42. Eukaryot Cell 1, 469–480.
Stevenson BJ, Ferguson B, De Virgilio C Bi E, Pringle JR, Ammerer G, Sprague GFJ (1995). Mutation of *RGA1*, which encodes a putative GTPase-activating protein for the polarity-establishment protein Cdc42p, activates the pheromone-response pathway in the yeast Saccharomyces cerevisiae. Genes Dev 9, 2949–2963.
Tong Z, Gao X-D, Howell AS, Bose I, Lew DJ, Bi E (2007). Adjacent positioning of cellular structures enabled by a Cdc42 GTPase-activating protein mediated zone of inhibition. J Cell Biol 179, 1375–1384.
Zheng Y, Bender A, Cerione RA (1995). Interactions among proteins involved in bud-site selection and bud-site assembly in Saccharomyces cerevisiae. J Biol Chem 270, 626–630.